香港氣象學會

HONG KONG METEOROLOGICAL SOCIETY

Bulletin

Volume 12, Numbers 1/2, 2002
ISBN: 1024-4468

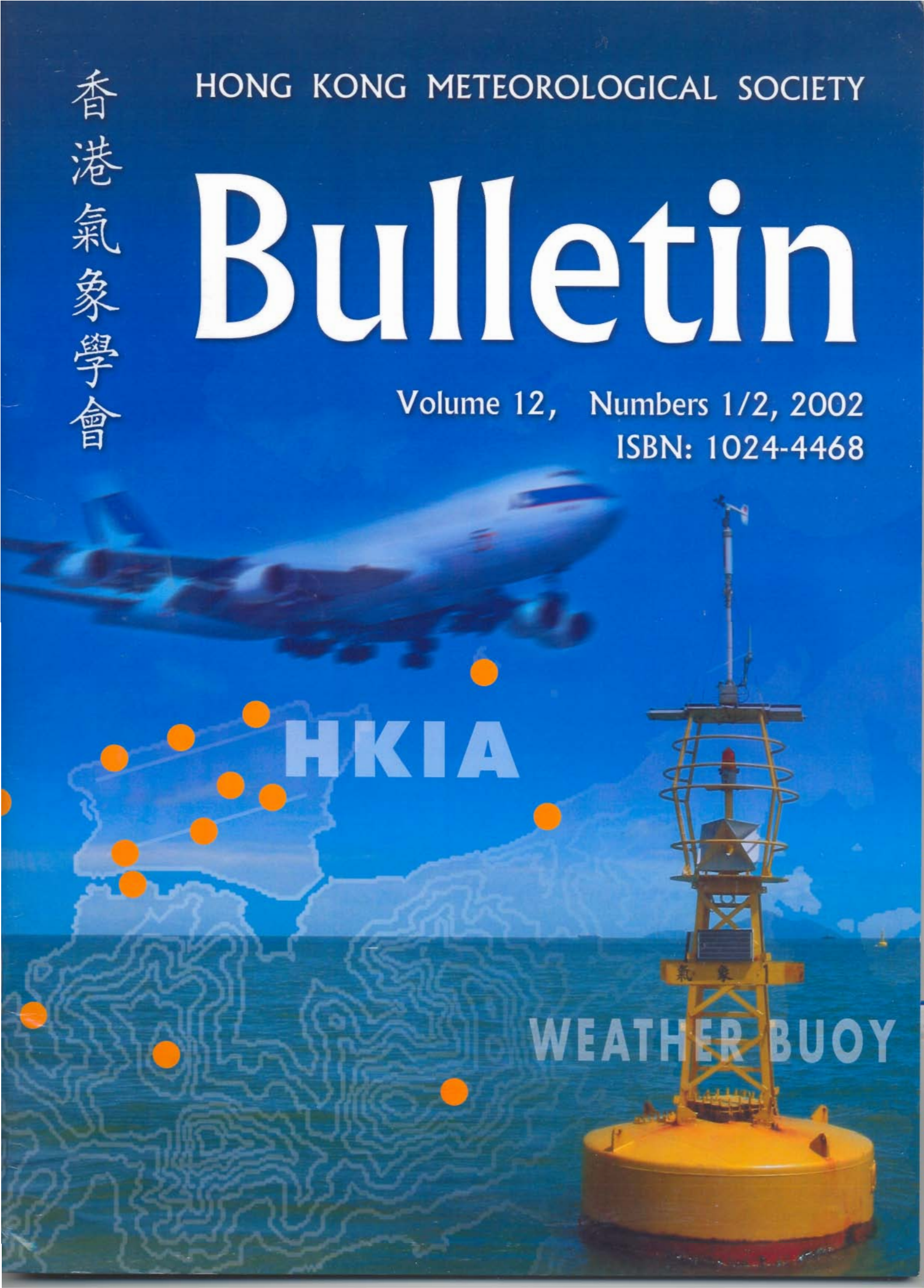

ISSN 1024-4468

The Hong Kong Meteorological Society Bulletin is the official organ of the Society, devoted to articles, editorials, news and views, activities and announcements of the Society.

Members are encouraged to send any articles, media items or information for publication in the Bulletin. For guidance see the "information for contributors" in the inside back cover.

Advertisements for products and/or services of interest to members of the Society are accepted for publication in the BULLETIN.

For information on formats and rates please contact the Society secretary at the address opposite.

Views and opinions expressed in the articles or any correspondence are those of the author(s) alone and do not necessarily represent the views and opinions of the Society.

The mention of specific products and/or companies does not imply there is any endorsement by the Society or its office bearers in preference to others which are not so mentioned.

SUBSCRIPTION RATES (Two issues per volume)

Institutional rate: HK$ 300 per volume

Individual rate: HK$ 150 per volume

Published by

The Hong Kong Meteorological Society

c/o Hong Kong Observatory
134A Nathan Road
Kowloon, Hong Kong

香港氣象學會

HONG KONG METEOROLOGICAL SOCIETY

Bulletin

Volume 12, Numbers 1/2, 2002

CONTENTS

Editorial

This issue of the Bulletin combines two issues in one volume and contains five papers all by staff of Hong Kong Observatory. These papers have been presented recently at conferences and are presented here in the interests of making their content more readily available to local readers.

The first paper by C.M Cheng, Queenie C.C. Lam and Edwin S.T. Lai provides a three-dimensional analysis of a mesoscale convective system over southern China and its role in the development of a localized rainstorm in Hong Kong. Their analysis identifies the factors contributing to the occurrence of localized heavy rain in this event and on that basis presents a schematic three-dimensional structure of the rainstorm.

In the second paper S.Y. Lau describes the enhancement of the low-level windshear and turbulence detection and alerting service in use at Hong Kong International Airport which involves advanced meteorological systems. These include the Terminal Doppler Radar (TDWR), two wind profilers and a network of anemometers.

The third paper by Y.K. Leung and W.M. Leung focuses on the effect of ENSO on the number of tropical cyclones affecting Hong Kong. Results from studies carried out to identify the interannual variation of tropical cyclone activity in the western North Pacific Ocean, indicate that the interannual variation in tropical cyclone activity is related to the El Niño-Southern Oscillation (ENSO) phenomenon. Their paper investigates if and how this variability influences the number of tropical cyclones affecting Hong Kong.

In the fourth paper T.C. Lee and W.M. Leung examines the performance of multiple-model ensemble techniques for predicting tropical cyclone tracks. Results indicate that the method using the EW scheme outperformed all individual models in TC track prediction in 1999-2001. Reductions in 24-, 48-, and 72-hour forecast errors are about 7 percent, 17 percent and 19 percent respectively. Use of the method results in significant improvement of the performance of HKO's official TC forecast. Further improvements in performance of the ensemble forecast are possible by use of a different weighting scheme based on the 12-hour forecast position errors of individual members of the ensemble.

The last paper by P.W. Chan and K.K. Leung reports on the experimental use of a weather buoy for windshear monitoring at the Hong Kong International Airport.

This issue of the Bulletin represents my last as Editor-in-Chief. During the past 12 years I have been grateful for the contributions of members and the assistance of those who have served on the Editorial Board. I will remain on the Editorial Board, and wish to convey my best wishes to the new Editor-in Chief, Y.K. Chan, for continuing success in this important endeavour on behalf of the Society.

Bill Kyle, Editor-in-Chief

Cho-Ming Cheng, Queenie Ching-Chi Lam & Edwin S. T. Lai

Hong Kong Observatory, 134A Nathan Road, Kowloon, Hong Kong

Three-dimensional Analysis of Mesoscale Convective System on 24 May 1998

Abstract

Rainstorms associated with an un-seasonal cold front affected the Pearl River Estuary on 24 May 1998, bringing a deluge of over 300 millimeters of rainfall to Hong Kong. Prior to the arrival of the cold front, intense rain echoes already developed in the prevailing unstable south to southeasterly airstream. The fast southeastward advancement of the cold front triggered off lifting of warm and moist air, thereby enhancing rain development along the front. Analysis of raingauge data suggested the heavy rain was concentrated in small pockets over a relatively confined region near the Pearl River Estuary.

Synoptic analyses based on TLAPS grid data prepared by the Guangzhou Regional Meteorological Center for SCSMEX suggested a favourable large-scale environmental setting for heavy rain development *viz*., intense low level convergence along the cold front, approach of mid-level troughs and existence of upper level divergence.

An analysis of radar reflectivity information and Doppler velocity data also identified mesoscale features conducive to the development of rainstorms within a relatively confined region. A mesocyclone near the coast of western Guangdong could be related to the occurrence of heavy rain near Hong Kong. The south to southwesterly winds of the mesocyclone converged with the northerly winds behind the cold front, creating intense low-level convergence on the eastern side of the mesocyclone near Hong Kong. Such convergence above the cold front was also evident on Doppler radar images. Based on numerical model analysis as well as radar observation, a schematic three-dimensional structure of the mesoscale convective system is presented.

Numerical model prediction of the rainstorm event by the Operational Regional Spectral Model (ORSM) of the Hong Kong Observatory is examined. Intense observations collected during SCSMEX were used to initialize the model. Model results suggested strong vertical motion associated with lifting of air above the cold front. The performance of the model in predicting the localized heavy rain and the mesoscale features associated with the rainstorm is reviewed.

Introduction

During the South China Sea Monsoon Experiment (SCSMEX), an unseasonal cold front formed over southern China and moved south to bring heavy rain to the Pearl River Estuary on 24 May 1998. The cold front swept across Hong Kong between 03 UTC and 07 UTC. More than 300 millimeters of rain fell over Hong Kong that day (Figure 1). In southern China, the heavy rain was concentrated over a relatively confined region near the Pearl River Estuary. In the six hours from 00 UTC to 06 UTC on 24 May 1998, the Pearl River Estuary had more than 80 mm of rain while most parts of Guangdong and Guangxi recorded less than 10 mm of rain (Figure 2).

Figure 1 **Distribution of daily rainfall (in mm) in Hong Kong on 24 May 1998. More than 300 mm of rain were recorded over the northern part of Hong Kong.**

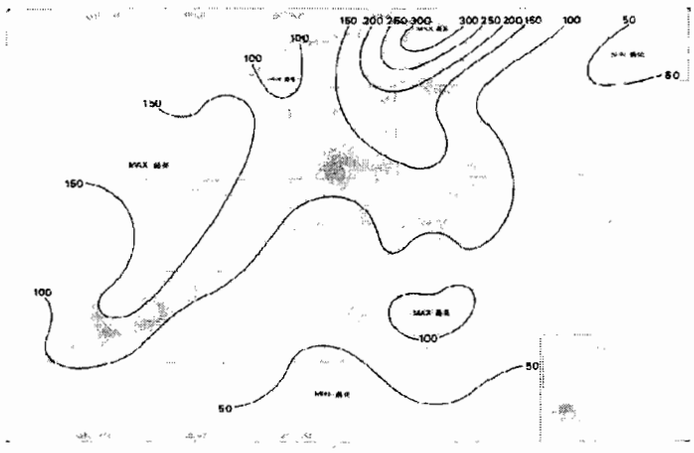

Figure 2 **Rainfall in excess of 80 mm was recorded near the Pearl River Estuary from 00 UTC to 06 UTC on 24 May 1998. Other parts of Guangdong and Guangxi generally received less than 10 mm of rain in the same period.**

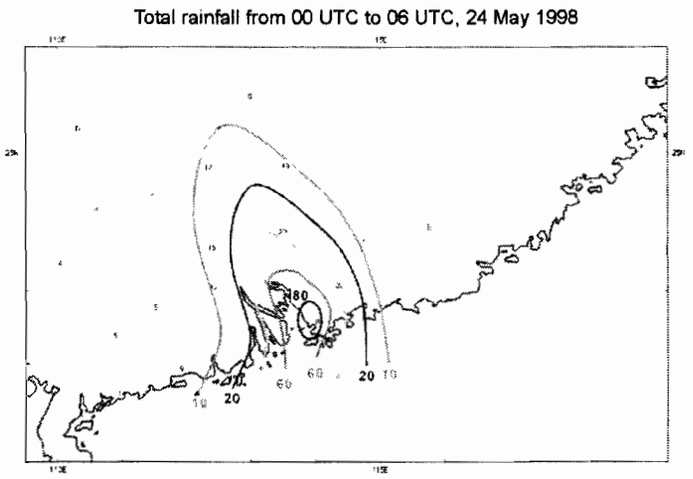

In the following section, an analysis based on TLAPS grid data prepared by the Guangzhou Regional Meteorological Center for SCSMEX is made to identify synoptic features favourable for heavy rain development. Radar data are also utilized to reveal mesoscale features conducive to the localized rainstorm development. Using intense observations collected during SCSMEX to initialize the Operational Regional Spectral Model (ORSM) of the Hong Kong Observatory, the performance of the model in predicting the localized heavy rain is reviewed.

Analysis of TLAPS Grid Data

(a) Surface level: ahead of tightly packed isobars, a cold front lying across southern China was pushed south to the coastal region (Figure 3). On the way south, the north to northwesterly winds associated with the cold front encountered the southeasterly airstream that prevailed near the Pearl River Estuary, thereby creating intense low-level convergence and lifting the moist air carried along by the southeasterly winds;

Figure 3 (a) A cold front lay across southern China at 12 UTC on 23 May 1998; (b) the cold front just moved past the Pearl River Estuary at 06 UTC on 24 May 1998.

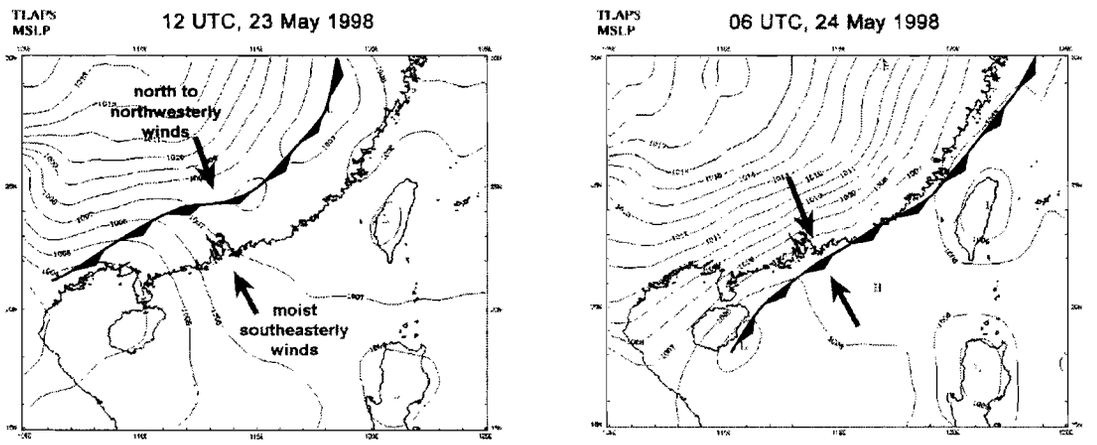

(a) (b)

Figure 4 (a) A trough at 700 hPa level reached western Guangdong at 12 UTC on 23 May 1998. (b) The 700 hPa level trough edged east closer to the Pearl River Estuary at 06 UTC on 24 May 1998. (c) A low-latitude trough at 500 hPa level reached western Guangdong at 12 UTC on 23 May 1998. (d) This 500 hPa level trough moved closer to the Pearl River Estuary at 06 UTC on 24 May 1998.

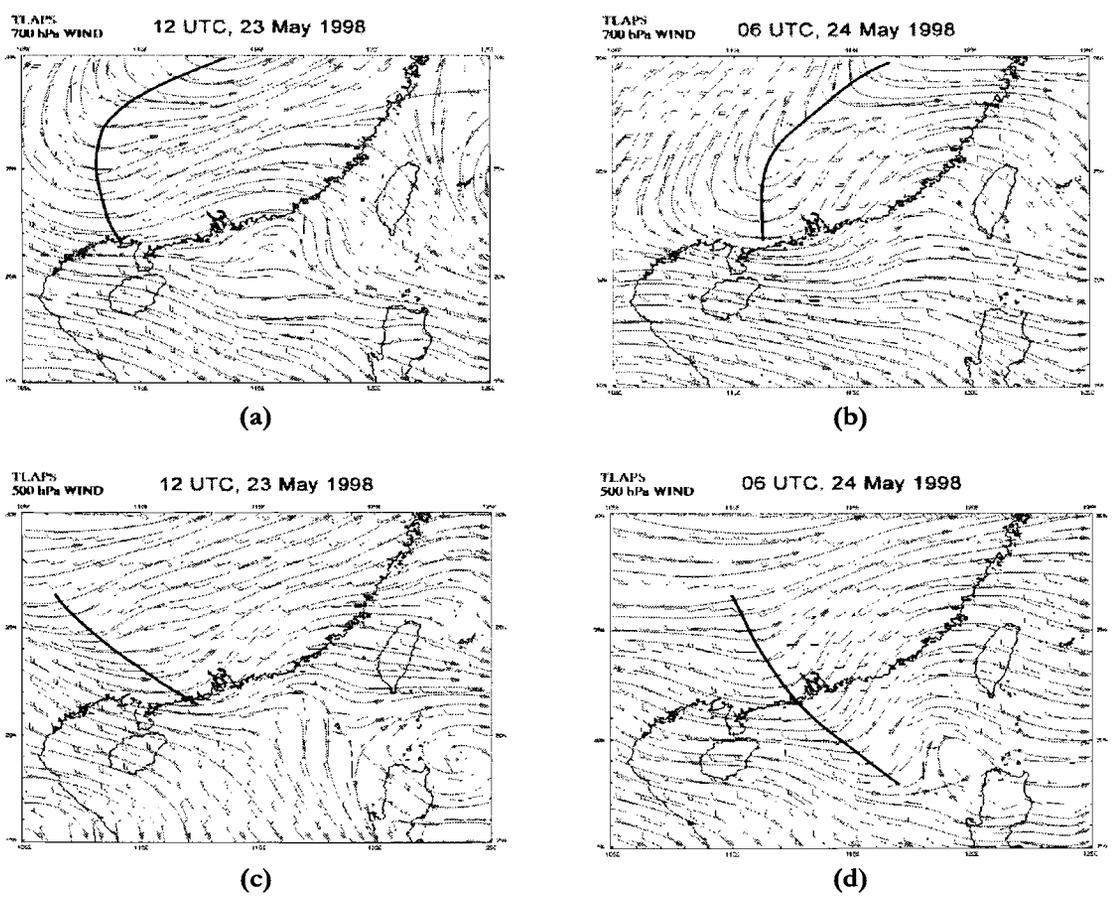

(a) (b)

(c) (d)

(b) Mid-levels: low-latitude troughs at 700 and 500 hPa levels approached the Pearl River Estuary from the west (Figure 4), favouring convective development in the region. The northwesterly winds behind the troughs also provided added momentum for the cold front to advance quickly southwards.

Figure 5 **(a) Broad anticyclonic flow covered southern China at 200 hPa level at 12 UTC on 23 May 1998. (b) A narrow ridge formed along the coastal region. The region of strong divergence spread south at 06 UTC on 24 May 1998, resulting in an increase in divergence over the Pearl River Estuary.**

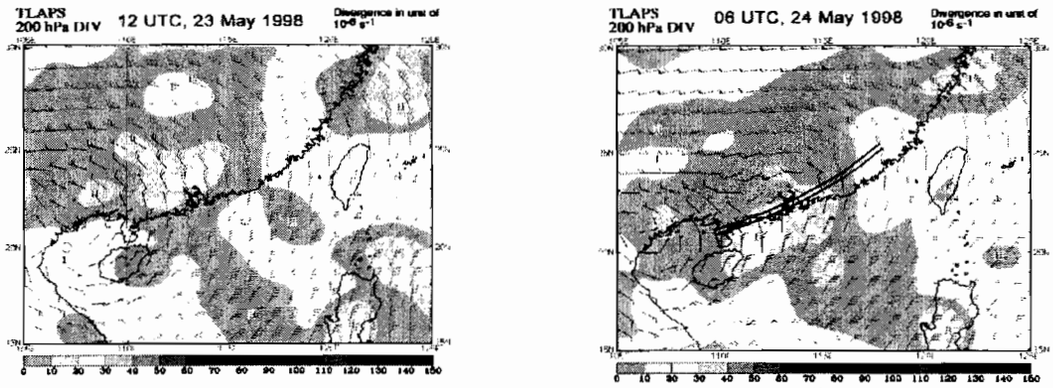

(a) (b)

(c) Upper level: against a background of broad anticyclonic flow over southern China, an area of strong divergence over inland Guangdong spread south to cover the Pearl River Estuary (Figure 5). Meanwhile, a narrow ridge formed and extended along the coastal region. This also favoured enhancement of convection near the coastal region.

Figure 6 **(a) Extensive area of convergence occurred along the southern boundary of the north to northeasterly winds at 925 hPa level at 12UTC on 23 May 1998. A mesocyclone was located over Beibu Wan. (b) A confined area of intense convergence covered the Pearl River Estuary while the mesocyclone moved close to the Pearl River Estuary at 06 UTC on 24 May 1998.**

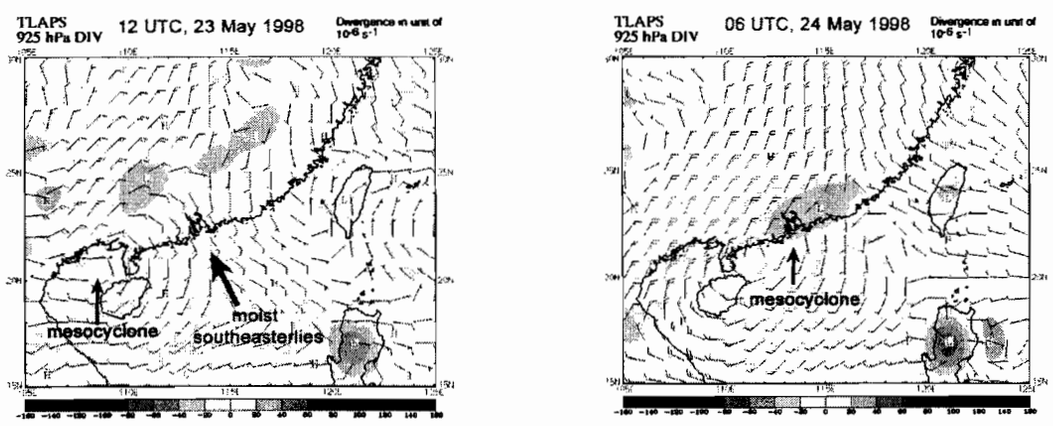

(a) (b)

TLAPS analyzed charts for 925 and 850 hPa levels revealed mesoscale features conducive to localized rainstorm development. At the 925 hPa level, intense convergence was apparent along the cold front.

A meso-α cyclone near Beibu Wan at 12 UTC on 23 May 1998 brought a stream of southerly winds that converged with the southeasterly winds from the northeastern part of the South China Sea, strengthening the winds over the Pearl River Estuary (Figure 6 (a)). While the trough associated with the cold front headed south to the coastal region, the mesocyclone moved closer to Hong Kong. Further enhancement of convergence occurred and a confined region of intense convergence covered the Pearl River Estuary at 06 UTC on 24 May 1998 (Figure 6 (b)).

Figure 7 **(a) Extensive area of convergence covered southern China at 850 hPa level at 12UTC on 23 May 1998 when a mesocylcone was located in Guangxi. (b) The area of convergence spread south towards the coast at 06 UTC on 24 May 1998. A localized region of strong convergence appeared to the north of the Pearl River Estuary. Meanwhile the mesocyclone moved close to Hong Kong.**

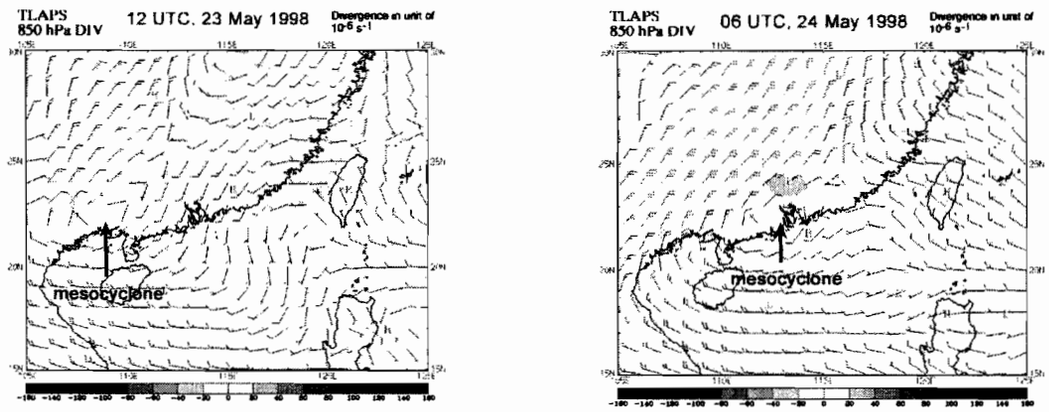

At 850 hPa level, a similar mesocyclone was located over Guangxi at 12 UTC on 23 May 1998 (Figure 7 (a)) about 200 km north of the mesocyclone at 925 hPa level. Again, this mesocyclone moved close to the Pearl River Estuary as the trough associated with the cold front reached the coastal region at 06 UTC on 24 May 1998 (Figure 7 (b)). Convergence was enhanced to the north of the Pearl River Estuary and the convergence value near Hong Kong also increased. At this time, the separation between the mesocyclone at 925 hPa and the mesocyclone at 850 hPa level decreased to less than 100 km.

Figure 8 **The tracks of the mesocyclones at 925 and 850 hPa levels. Separation between the two mesocyclones decreased on their way towards the Pearl River Estuary.**

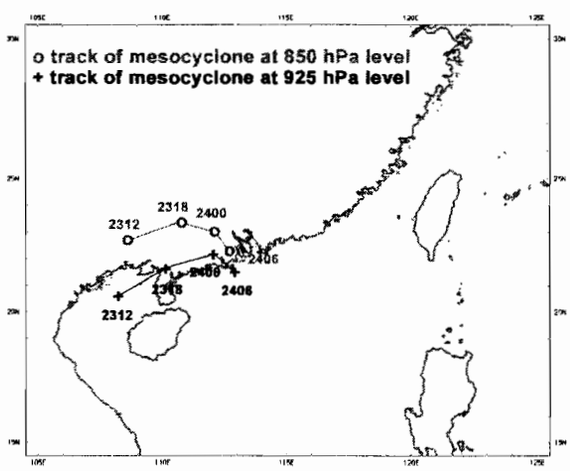

The mesocyclone played a key role in creating a region of localized intense convergence on the eastern side of the circulation, where an active southerly airstream converged with the north to northeasterly airstream behind the cold front. As the separation distance between the mesocyclones at 925 and 850 hPa levels shortened on their approach to the Pearl River Estuary at 06 UTC on 24 May 1998 (Figure 8), the overall low-level convergence near Hong Kong continued to increase. Without the mesocyclones, it was possible that the region of convergence would not have been so localized and intense.

Radar and Upper Air Sounding Analysis

The localized nature of the rainstorm could be readily seen on the radar images. Figure 9(a) illustrates the reflectivity image captured by a radar in Hong Kong at 04:30 UTC (12:30 Hong Kong Time) on 24 May 1998 at 1 km level. The rainstorm manifested itself as a narrow, north-south oriented rainband that approached the Pearl River Estuary from the west. The region of intense rain in excess of 30 mm h^{-1} in orange to red colours was generally less than 50 km in width and extended over a length of more than 150 km. As the rainband tracked east, individual rain echo moved north along the rainband.

Figure 9 **(a) Reflectivity image at 1 km level shows a narrow rainband in north-south orientation covering Hong Kong at 04:30 UTC (12:30 Hong Kong Time) on 24 May 1998. (b) Doppler velocity image indicated convergence of prevailing southerly winds with northwesterly winds of the cold front.**

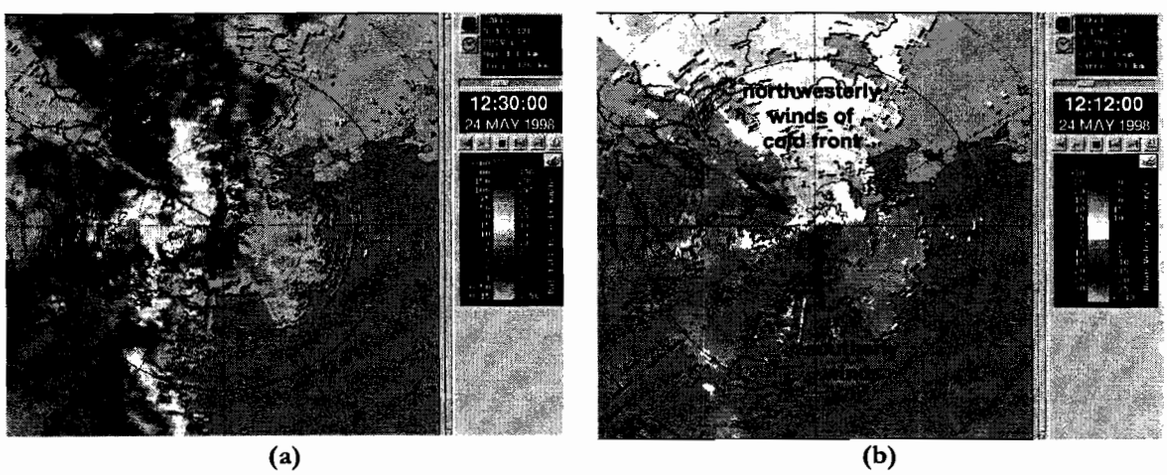

(a) (b)

The Doppler velocity image at 04:30 UTC is depicted in Figure 9(b). The prevailing flow over the radar site was southerly. Meanwhile, northwesterly winds behind the cold front reached the western part of Hong Kong, converging with the prevailing southerlies. Combining the reflectivity image and the Doppler velocity image, it was found that intense echoes already developed within the prevailing southerlies. Arrival of the cold front triggered off enhanced convective development, leading to the heavy rain event.

Low level convergence of the cold front with the prevailing southerlies is clearly discernible in the vertical cross-sectional images. Figure 10 contains the vertical cross-sections along the line AB as shown in Figure 9(a). Point B is the location of the radar. Intense rain echoes were observed along the leading edge of the cold front about 10 km from the radar site (Figure 10(a)). Behind the cold front, rain echoes overshot to above 10 km in height. The Doppler velocity image (Figure 10(b)) showed convergence of approaching echoes associated with the cold front in green colour, with the receding echoes in yellow and orange colours near the radar site. The boundary between the two regions corresponded to the frontal slope, which appeared to be rather steep below 2 km height. This boundary flattened off and appeared wavy between 2 and 4 kilometres in altitude, typical of shear gravity wave (or Kelvin-Helmholtz wave) on frontal surface (Fleagle 1980).

The Spectrum width image (Figure 10(c)) revealed broad spectrum width along the steep frontal boundary and along the shear gravity wave region, consistent with the turbulent nature in these two regions.

Figure 10 **Vertical cross-sections along line AB in Figure 9(a). (a) reflectivity image indicated intense convection forming near the frontal boundary about 10 km from the radar site; (b) Doppler velocity image illustrated strong convergence on the frontal boundary at low level. Shear gravity wave feature appeared between 2 and 4 km levels; (c) Broad spectrum width occurred along the frontal boundary and in the shear gravity wave region, suggestive of turbulence there.**

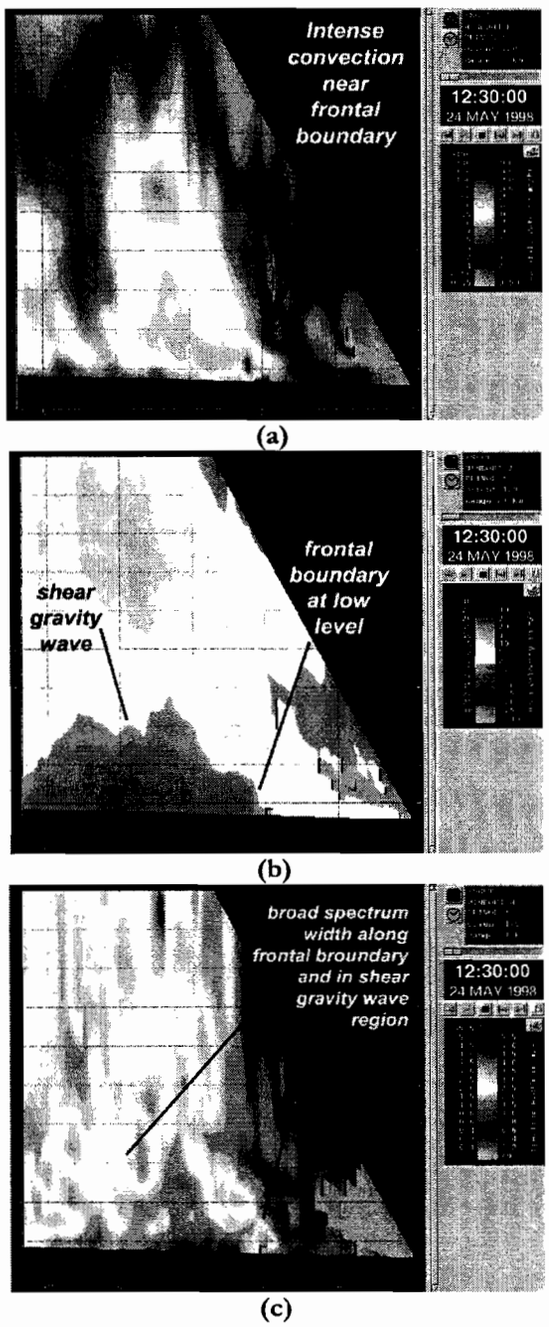

Figure 11 **(a) Tephigram at 00 UTC on 24 May 1998 indicated moist atmosphere from surface up to 300 hPa level. Warm advection in the atmosphere was also apparent in the upper air sounding data. (b) At 06 UTC on 24 May 1998, the atmosphere remained very humid. Cold advection at the wake of the cold front was discernible between 3 and 7 km levels.**

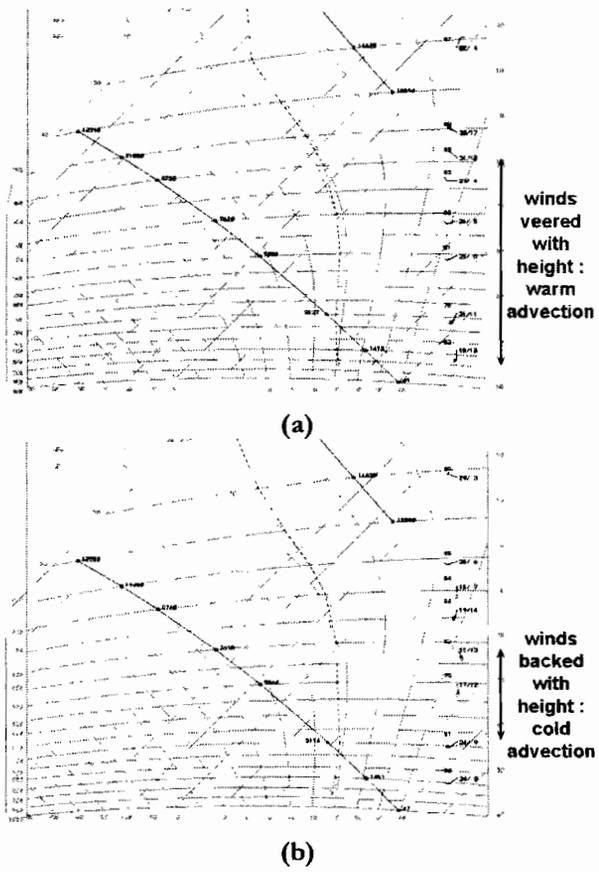

Before the arrival of the cold front, the tephigram for Hong Kong at 00 UTC on 24 May 1998 (Figure 11(a)) revealed an unstable and very humid atmosphere from surface up to 300 hPa level. The upper air sounding data indicated warm advection in the lower and middle troposphere signified by veering of winds with height. After the passage of the cold front over the upper air sounding station at 06 UTC on 24 May 1998 (Figure 11(b)), the atmosphere remained very humid. Cold advection was apparent between 3 and 7 km levels, where winds backed with height.

Numerical Model Result

Numerical model prediction of the rainstorm event was performed on the Operational Regional Spectral Model (ORSM) of the Hong Kong Observatory. The ORSM is a hydrostatic model with nested grids at 20 km and 60 km horizontal resolution and with 36 vertical layers. Intense observations at 21 UTC on 23 May 1998 during SCSMEX were used to initialize the model. Previous study revealed that the inclusion of intense observations improved the radar rainfall analysis used in the physical initialization of the ORSM and increased the forecast rainfall amount on 24 May in the Guangdong region north of Hong Kong (Wong *et. al.*, 2000). The model prediction for 06 UTC on 24 May 1998 is shown in Figure 12. It shows that the packed pressure gradient had already reached the south China coast (Figure 12(a)), consistent with the TLAPS analysis in Figure 3(b). Forecast pressure to the south of the Pearl River Estuary was however a little lower than that in the TLAPS analysis. The 6-hourly accumulative rainfall pattern agreed quite well with the observation in Figure 2.

Figure 12 **Model prediction of rainstorm event at 06 UTC on 24 May 1998 by ORSM based on intense observations at 21 UTC on 23 May 1998.**

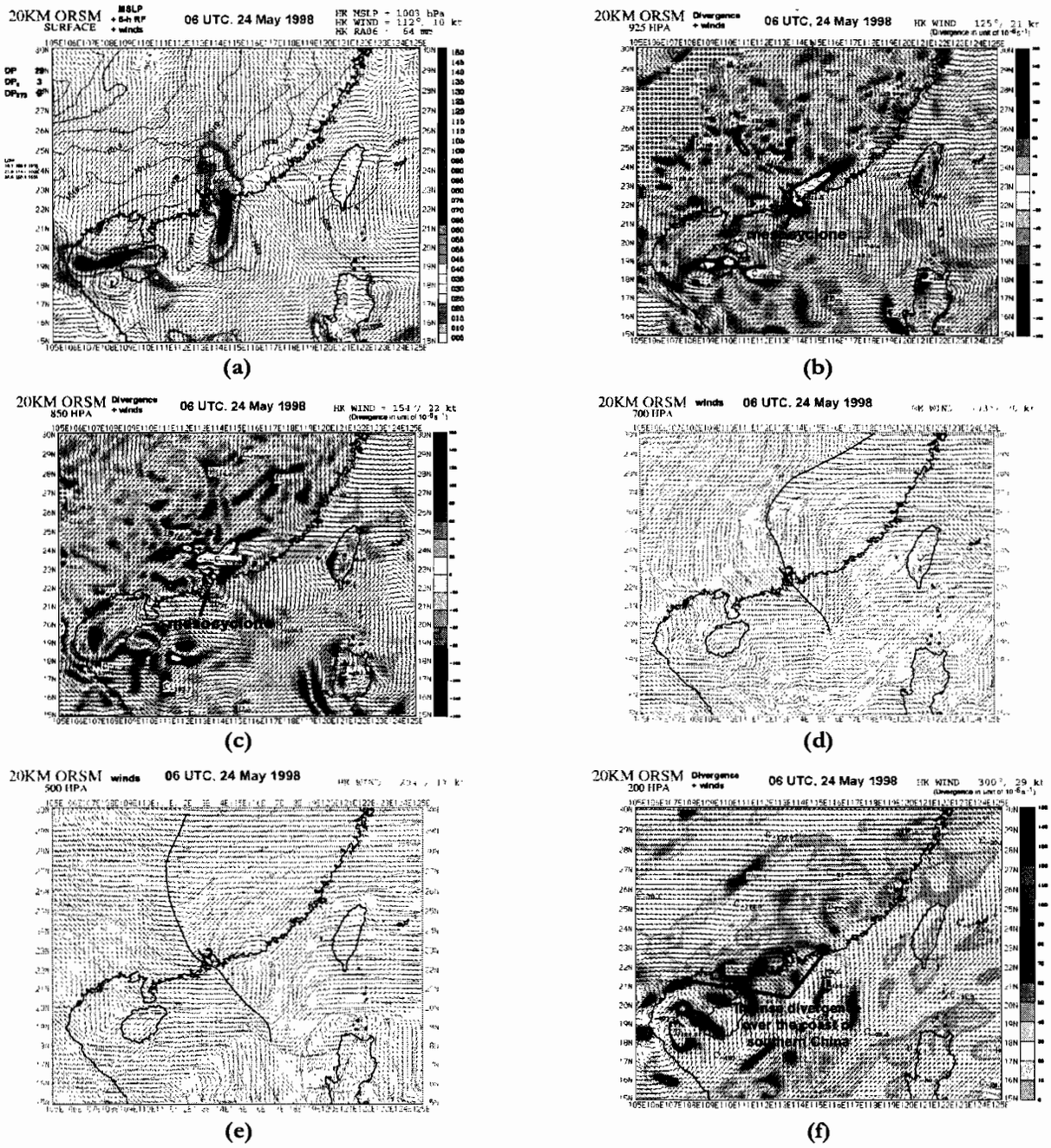

The mesocyclone near the Pearl River Estuary at 925 and 850 hPa levels was well forecast by the model (Figure 12(b) and 12(c)). The location of intense convergence associated with the mesocyclones also agreed very well with the TLAPS analysis. The high convergence value was consistent with the occurrence of heavy rain near Hong Kong, even though the predicted convergence from ORSM was apparently higher than that in the TLAPS analysis owing to the difference in grid spacing.

At 700 hPa level (Figure 12(d)), the trough near the Pearl River Estuary and over the northern part of the South China Sea was sharper than that in the TLAPS analysis. At 500 hPa level (Figure 12(e)), the distinct northwest-southeast oriented trough over southern China was very well captured by the model. At 200 hPa level (Figure 12(f)), while the ridge axis along the coast of southern China was never as sharp as in the TLAPS analysis, the model did predict significant divergence along the coastal region and conditions favourable for rainstorm development.

Figure 13 **(a) Vertical cross-section across the cold front showing model prediction by ORSM for 06 UTC on 24 May 1998. Strong vertical motion of air above the cold front is apparent. (b) Vertical cross-section along the cold front indicated a narrow column of positive vorticity. The region of strongest positive vorticity is associated with the mesocyclone at 925 hPa level.**

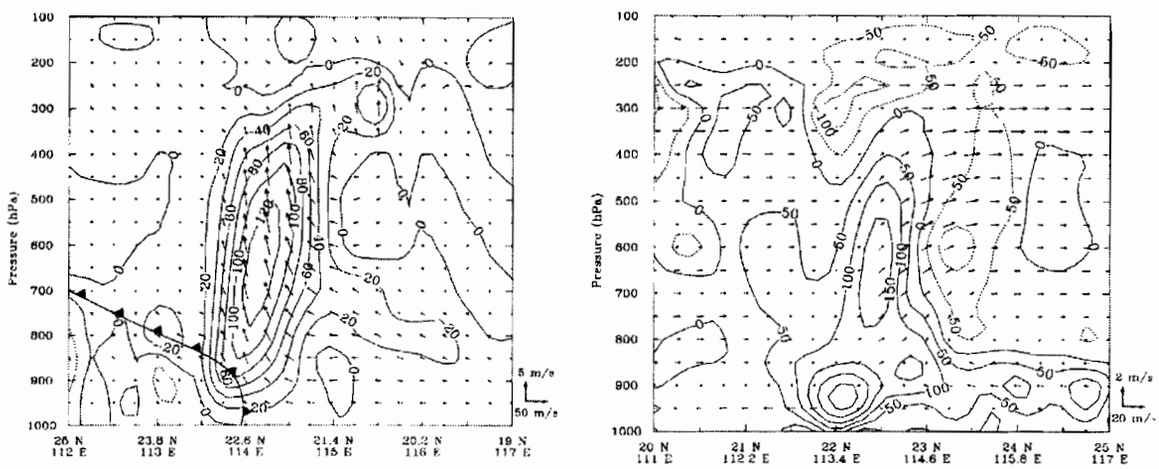

(a) (b)

A vertical cross section across the cold front is presented in Figure 13(a). It shows a region of strong vertical motion associated with air lifted above the cold front leading to the heavy rainstorm. The vertical cross section along the cold front (Figure 13(b)) indicates a narrow, vertical column of intense vorticity that extended from surface up to 400 hPa level. The maximum vorticity was found at 925 hPa level and was associated with the mesocyclone at this level. It is believed that the localized nature of the rainstorm in the vicinity of Hong Kong were directly related to the mesocyclone in the lower troposphere, causing strong convergence and therefore strong vertical motion within a confined region.

Conclusion

From the above analyses, it was found that the synoptic weather conditions over southern China were conducive to heavy rain development, *viz.*, occurrence of convergence at low levels, approach of mid-level troughs at 700 and 500 hPa levels, and increased upper air divergence from a narrow ridge at 200 hPa level. There were a number of factors contributing to the occurrence of localized heavy rain: (a) a stream of moist southeasterly winds near the surface passing right over the Pearl River Estuary and converging with the north to northeasterly winds behind the surface cold front; (b) the mesocyclone at 925 and 850 hPa levels drew in southerly winds over the Pearl River Estuary, that converged with the approaching north to northeasterly winds behind the cold front at these levels. As a result, low level convergence was enhanced within a confined region near Hong Kong leading to the development of localized rainstorms. Without the mesoscale features observed, heavy rain would probably not have been so localized and intense. Based on these analyses, a schematic three-dimensional structure of the mesoscale rainstorm is presented in Figure 14.

Figure 14 **A schematic diagram showing the three dimensional structure of the localized rainstorm near the Pearl River Estuary.**

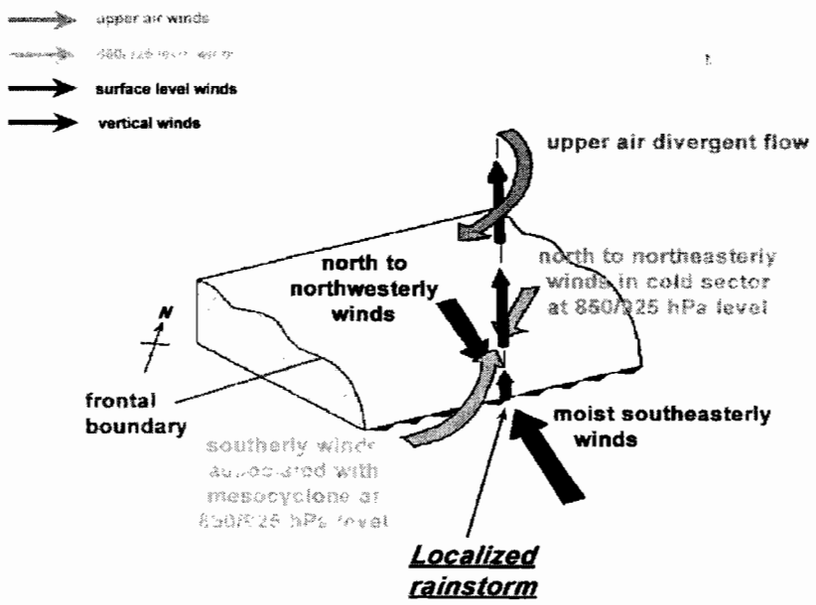

Acknowledgement

The authors would like to thank Mr. C.K. Chow for preparing the charts of TLAPS analysis and ORSM model. The material presented in this paper was originally presented at the *Scientific Conference on the South China Sea Monsoon Experiment (SCSMEX)* held in Shanghai, China from 17-20 April, 2001.

References

Fleagle, R.G. and Businger, J.A. (1980) *An Introduction to Atmospheric Physics, Second Edition*, Academic Press.

Wong, W.K. and Lam, Hilda (2000) *Impact of Mesoscale Observation Data on Forecasting the Rainfall Event on 24 May 1998 by the Regional Spectral Model*, presented at *Conference on Monsoon and Rainstorm*, Zhuhai, China, 11-12 April 2000.

S.Y. Lau

Hong Kong Observatory, 134A Nathan Road, Kowloon, Hong Kong

Windshear and Turbulence Detection and Warning at Hong Kong International Airport

With the re-location of the Hong Kong International Airport (HKIA) from Kai Tak to Chek Lap Kok, the aviation meteorological service provided by the Hong Kong Observatory (HKO) underwent a major modernization programme. A key component of the programme was the enhancement of its low-level windshear and turbulence detection and alerting service. As part of this enhancement programme, advanced meteorological systems, including inter alia the Terminal Doppler Weather Radar (TDWR), two wind profilers and a network of anemometers were deployed. The location of the various meteorological sensors is given in Figure 1. Data from these equipment are then ingested and processed by computer to provide an integrated windshear and turbulence alert for the airport.

The TDWR is strategically located at Tai Lam Chung about 12 km northeast of HKIA for detecting microbursts and windshear associated with convection. The TDWR has a clear view of the runways, as well as airport approach and departure areas. To avoid beam blockage by ships, the antenna of the TDWR is situated at about 60 m amsl.

Apart from the TDWR, the differences in wind measured at adjacent anemometers over the airport are used to infer the location and magnitude of the horizontal windshear in the approach and departure corridors similar to the Low-level Windshear Alert System (LLWAS) used in airports over USA. A number of anemometers are also located on hill tops on Lantau Island to measure the ambient wind speed and direction and their fluctuations, from which the magnitude and location of the terrain-induced windshear and turbulence is inferred by the correlation method.

The wind profilers at Sha Lo Wan and Siu Ho Wan monitor the vertical profile at the western and eastern approach respectively. The profilers measure the lower troposphere continuously allowing the vertical profile to be updated every 10 minutes.

Data from all the equipment are fed into a computerised data processing system where the data are integrated to give a coherent alert based on all data sources. Since the airport opened, windshear and turbulence associated with thunderstorms, low level jets, sea breezes, surges of winter monsoon and terrain have been observed. The facilities, in particular the TDWR, put in place by the HKO have proved to be very useful in observing the windshear phenomena and contribute towards enhancing the windshear alerting service at HKIA.

Figure 1 Map of HKIA and its surrounding areas. Terrain contours are given in 100 m intervals.

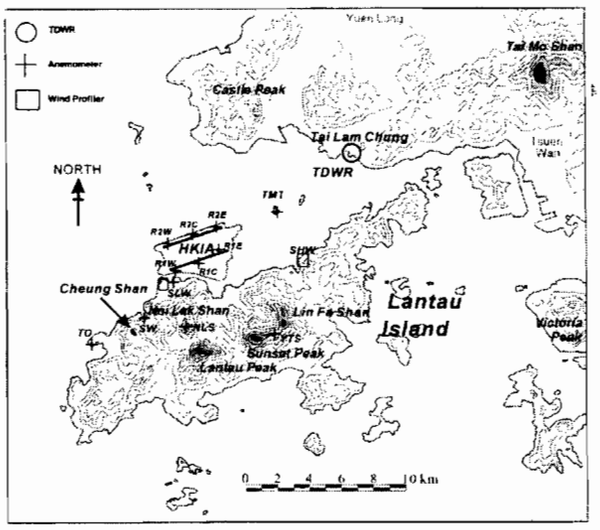

Apart from automatic alerts from the equipment, the aviation forecasters remain vigilant about the weather situation and issue alerts to complement those from the equipment. A knowledge base on the occurrence of windshear has been developed using pilot reports to support aviation forecasters in issuing these complementary windshear alerts. Aviation forecasters also issue alerts based on pilot reports in accordance with ICAO Annex 3.

The TDWR is highly sensitive and is able to determine the radial velocity under some non-rainy conditions. However, when the weather is fine, the return signal may be just too weak for the TDWR to determine the wind field for windshear detection. The HKO is also in the process of acquiring a coherent pulsed Doppler LIDAR to study the detection of terrain-induced windshear in clear air conditions.

With the introduction of the new suite of meteorological equipment for windshear detection, a major effort was expanded on the training of forecasting personnel, air traffic controllers and maintenance personnel. Emphasis was also placed on informing pilots how the system works and about the meaning of the alerts. This included a large-scale briefing to inform the users of the characteristics of terrain-induced windshear and turbulence at HKIA, promulgating the information in the Aeronautical Information Publication (AIP) and the publication of a brochure on "Windshear and Turbulence Detection for the new airport at Chek Lap Kok". The HKO also worked with the Hong Kong Airline Pilots Association to publish a special supplement on "Windshear & Turbulence Alert! - Windshear Alert and Turbulence Systems at Chek Lap Kok". Apart from the above publications, information on the windshear and turbulence alerting service at HKIA is also available on the Aviation Meteorological Information Dissemination System (AMIDS) to facilitate access by users. As a public awareness programme, pamphlet on windshear and turbulence has been published while general information on the windshear and turbulence alerting service at HKIA is also available in the HKO web site (http://www.weather.gov.hk/aviat/amt_e/amsmain_e.htm).

Acknowledgement

The material presented in this paper was originally presented in the 13th *Newsletter of the Working Group on Training, the Environment and New Developments (TREND)*, of the Commission for Aeronautical Meteorology, WMO, in July 2001.

Y.K. Leung and W.M. Leung

Hong Kong Observatory, 134A Nathan Road, Kowloon, Hong Kong

Effect of ENSO on Number of Tropical Cyclones Affecting Hong Kong

Introduction

A number of studies have been carried out to identify the interannual variation of tropical cyclone activity in various ocean basins. Results show that over the western North Pacific Ocean, the interannual variation in tropical cyclone activity is related to the El Niño-Southern Oscillation (ENSO) phenomenon (*e.g.* Chan 1985; Lander 1994). The aim of this study is to investigate if and how this variability influences the number of tropical cyclones affecting Hong Kong.

Data

In this study, forty years of tropical cyclone data (1961-2000) from the Hong Kong Observatory are used. The number of tropical cyclones affecting Hong Kong is defined as the number of tropical cyclones necessitating the issuance of tropical cyclone warning signal for Hong Kong. When a tropical cyclone is within 800 km from Hong Kong (Figure 1) and may affect Hong Kong, the Hong Kong Observatory will issue a tropical cyclone warning signal to warn the local public.

Sea surface temperature and the large-scale upper air data are extracted from the re-analysis data of the United States National Center of Environmental Protection (NCEP). These re-analysis data are grid data with a horizontal resolution of 2.5° x 2.5°. A detailed description of NCEP re-analysis data can be found in Kalnay (1996).

Figure 1. A location map showing the area of 800 km from Hong Kong

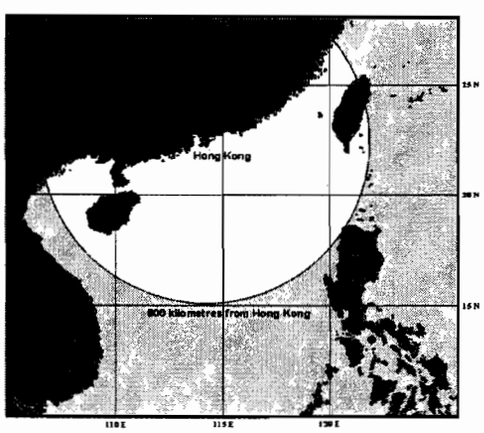

Variation of number of tropical cyclone affecting Hong Kong with Sea Surface Temperature Anomalies

As most studies suggest that sea surface temperature is closely related to tropical cyclone activity, the general pattern with which the sea surface temperature anomalies (SSTAs) over the tropical oceans is correlated to the annual number of tropical cyclone affecting Hong Kong (N) is examined. Figure 2 is a map showing the correlation between N and SSTAs in 2.5° x 2.5° grid over ocean areas. It can be seen that the strongest correlation between N and SSTAs occurs in the equatorial Central and Eastern Pacific, roughly coinciding with the four Niño regions, i.e., Niño-1+2, Niño-3, Niño-3.4 and Niño-4 (Figure 3).

Figure 2. Correlation between the annual number of tropical cyclones affecting Hong Kong and the annual sea surface temperature anomaly in various ocean basin. (Data period: 1961-2000, the colour scale represents values of correlation coefficients. Image is provided by the NOAA-CIRES Climate Diagnostic Center, Boulder, Colorado from the web site at http://www.cdc.noaa.gov/).

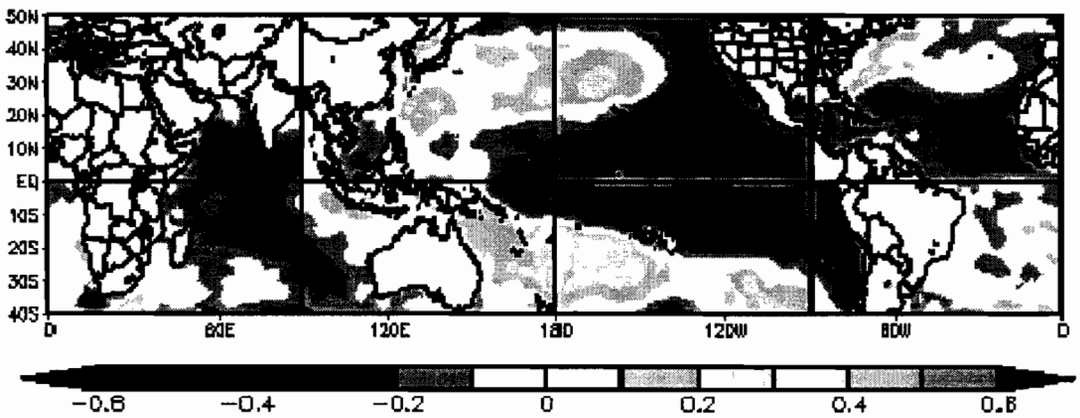

Figure 3. Location map of Nino-1+2, Nino-3, Nino-3.4 and Nino-4.

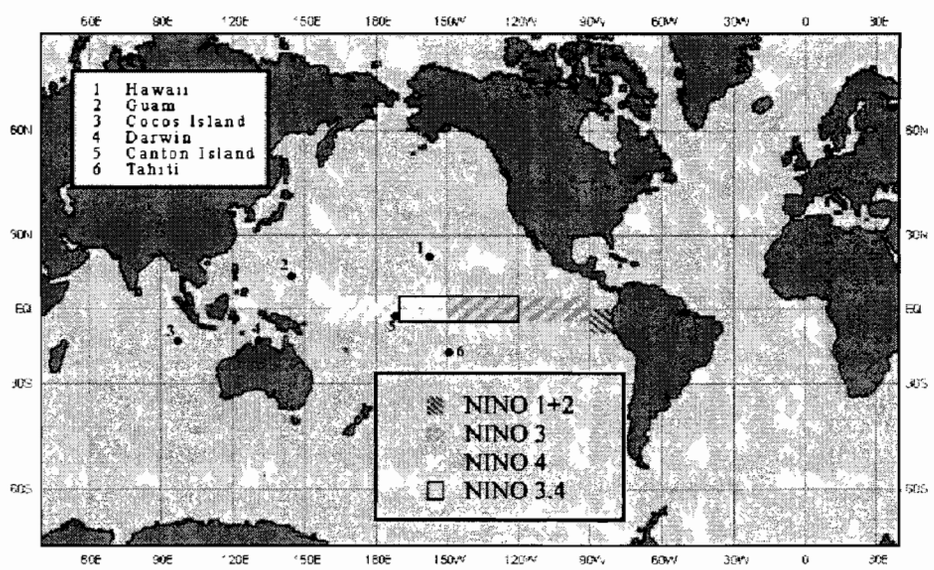

Table 1. **Correlation coefficients between the annual number of tropical cyclones affecting Hong Kong and the averaged annual sea surface temperature anomaly in various Niño regions.**

	Nino-1+2	Nino-3	Nino-3.4	Nino-4
Correlation coefficient	-0.39	-0.47	-0.47	-0.43

Table 1 shows the correlation between N and the mean annual SSTAs in each of the four Niño regions. While all of them are statistically significant at 0.05 level, the highest correlation occurs in Niño-3 and Niño-3.4. The Hong Kong Observatory has been using Niño-3.4 to classify ENSO events. The fact that the correlation of tropical cyclone number with SSTAs is highest in Niño-3.4 (as well as Niño-3) shows that this is an appropriate choice for studying the number of tropical cyclone affecting Hong Kong. In the 40-year period (1961-2000), there were occasions where SSTA in Niño-3.4 changed sign in the latter half of the year. In such cases, the SSTA in Niño-3.4 in the latter half of the year (the rainy and typhoon seasons in Hong Kong) is preferred over that of the first half of the year. Accordingly, the years 1965, 1969, 1972, 1976, 1982, 1983, 1986, 1987, 1991, 1992, 1994 and 1997 are El Niño years. The years 1964, 1970, 1971, 1973, 1974, 1975, 1988, 1989, 1995, 1998, 1999 and 2000 are La Niña years.

Figure 4. **Scatter diagram showing the relationship between the annual number of tropical cyclones affecting Hong Kong and the sea surface temperature anomaly in region Nino-3.4.**

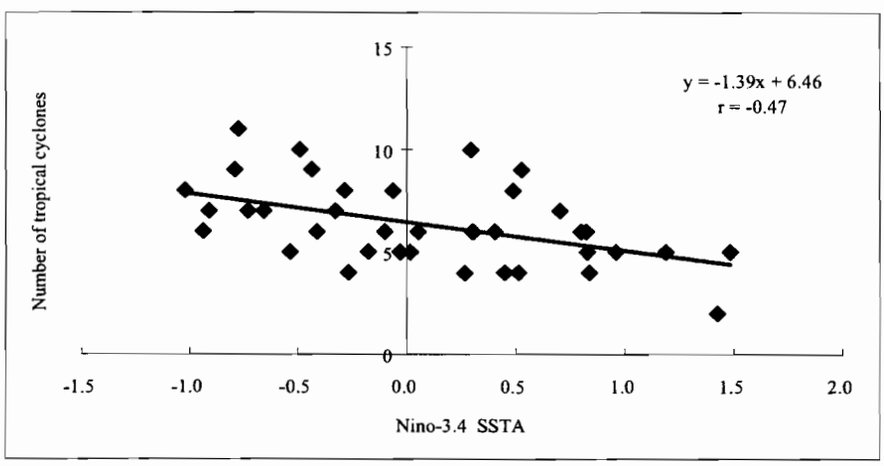

From the scatter diagram in Figure 4, it is seen that for warm phases of ENSO, N is relatively low while for cold phases of ENSO, N is relatively large.

The distribution of N for the 40 years (1961 - 2000) is shown in Figure 5. N ranges from 2 (in 1997, an El Niño year) to 11 (in 1974, a La Niña year), with a mean and standard deviation of 6.4 and 1.96 respectively. The Hong Kong Observatory takes N to be normal when it is within half of a standard deviation from the mean (i.e. within 6.4 ± 0.98). Taking integer values, a year is taken as having normal tropical cyclone activity when N is 6 or 7. N less than or equal to 5 will be taken as below normal, and N equal to or greater than 8 is taken as above normal. For El Niño or warm ENSO years, the average value of N is 4.8. Of the twelve El Niño years, nine have N below normal while the remaining three are normal. For La Niña or cold ENSO years, the average value of N is 7.8. Of the twelve La Niña years, six have N above normal, five are normal whereas the remaining year is below normal.

Figure 5. **Frequency distribution of the annual number of tropical cyclones affecting Hong Kong**

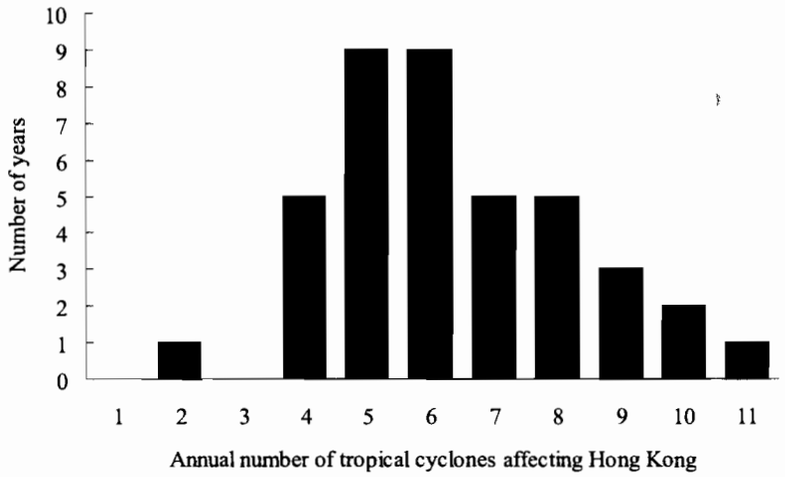

Table 2. **Annual number of tropical cyclones affecting Hong Kong for years of (a) EN-1 (b) EN(0) (c) EN+1 (d) LN-1 (e) LN(0) (f) LN+1 and (g) LN+2.**

(a) EN-1

Mean = 7.1 SD = 1.73	
Year	**Annual no. of tropical cyclones**
1964 (LN(0))	10
1968	6
1971 (LN+1)	9
1975 (LN+2)	7
1981	5
1985	5
1990	6
1993	9
1996	7

(b) EN(0)

Mean = 4.6 SD = 1.17	
Year	**Annual no. of tropical cyclones**
1965	6
1969	4
1972	5
1976	5
1982	5
1986	4
1991	6
1994	4
1997	2

(c) EN+1

Mean = 5.7 SD = 0.94	
Year	**Annual no. of tropical cyclones**
1983	7
1987	5
1992	5

(d) LN-1

Mean = 4 SD = 1	
Year	**Annual no. of tropical cyclones**
1963	4
1969 (EN(0))	4
1972 (EN(0))	5
1987 (EN+1)	5
1994 (EN(0))	4
1997 (EN(0))	2

(e) LN(0)

Mean = 7.3 SD = 1.80	
Year	**Annual no. of tropical cyclones**
1964	10
1970	6
1973	9
1988	6
1995	8
1998	5

(f) LN+1

Mean = 8.8 SD = 1.48	
Year	**Annual no. of tropical cyclones**
1971	9
1974	11
1989	7
1999	8

(g) LN+2

Mean = 7 SD = 0	
Year	**Annual no. of tropical cyclones**
1975	7
2000	7

To examine how N varies with the progress of ENSO events, the values of N prior to, during and after the onset of El Niño and La Niña events are listed in Table 2. EN-1 is the year prior to El Niño onset, EN(0) is the year of onset while EN+1 is the year after onset. LN-1, LN(0), LN+1 and LN+2 are similarly defined for La Niña years.

- In the nine EN-1 years, the mean value of N is 7.1. There are two years with N below normal, four years with normal N values and three years with N above normal. Of the three years with N above normal, two happen to be LN(0) or LN+1.
- In the nine EN(0) years, apart from two with normal N, all other have values of N below normal.
- For the three EN+1 years, one has normal N while the other two have N below normal.
- In six LN-1 years, all have N less than normal. It is noted, however, that five of these six years are either EN(0) or EN+1 years.
- For the six LN(0) years, one is having N less than normal, two are normal while the remaining three have N higher than normal.
- For the four LN+1 years, three of them have higher than normal N while one has normal N.
- For the two LN+2 years, the values of N are normal.

From the above, it can concluded that the annual number of tropical cyclones is predominantly less than normal for EN(0) years and EN+1 years. For LN(0) and LN+1 years, predominantly more tropical cyclones affect Hong Kong. No conclusion can be drawn for EN-1, LN-1 and LN+2 years.

Intermediate factors affecting tropical cyclone activity in Hong Kong

It is likely that ENSO events could affect tropical cyclone activity in Hong Kong by changing the location of tropical cyclone genesis and the steering current. These two aspects are investigated below.

Lander (1994) suggested that SSTAs are related to the longitudinal shift in the upward and downward branches of the Walker Circulation. Chen *et al.* (1998) further suggested a longitudinal variation of the monsoon trough in response to SSTAs. Such a shift would result in a corresponding shift of the tropical cyclone genesis locations. A plot of the mean tropical cyclone genesis locations in El Niño and La Niña years is given in Figure 6.

Figure 6. Mean tropical cyclone genesis location map for El Niño and La Niña years

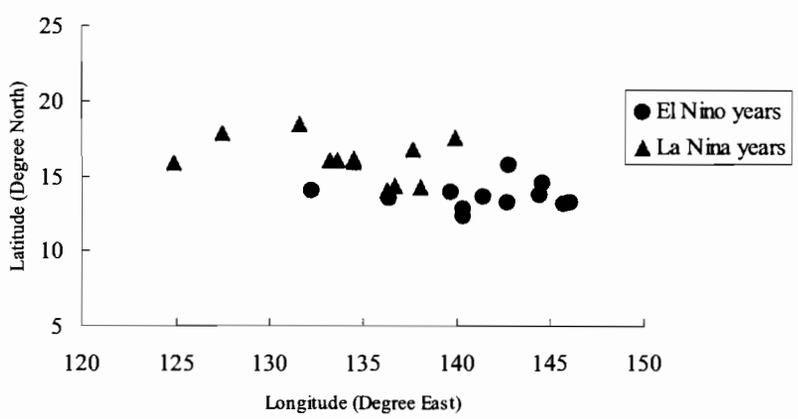

It shows that in general the genesis positions are shifted to the east in El Niño years as compared to La Niña years. When tropical cyclones form further east, they are more likely to interact with mid-latitude systems and recurve to the north before entering the South China Sea (SCS) to affect the south China coast and Hong Kong. Vice-versa, when tropical cyclones form further to the west in La Niña conditions, chances of their entering the SCS to affect Hong Kong are relatively high.

Figure 7. **500 hPa vector wind anomaly composite maps in fall for years with N (a) less than 6 (b) greater than 7. (The arrow indicates the direction of wind anomaly and the colour scale represents the magnitude of wind anomaly in ms^{-1}. Image is provided by NOAA-CIRES Climate Diagnostic Center, Boulder, Colorado from the web site at http://www.cdc.noaa.gov/).**

(a) Years with N below normal (N < 6)

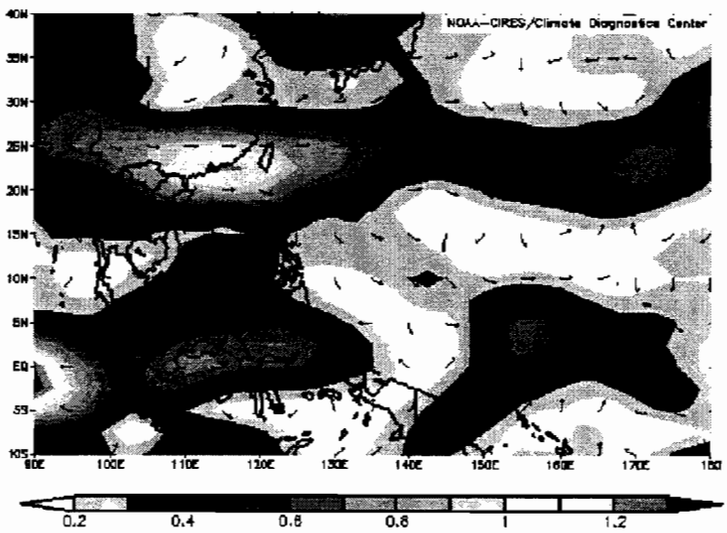

(b) Years with N above normal (N > 7)

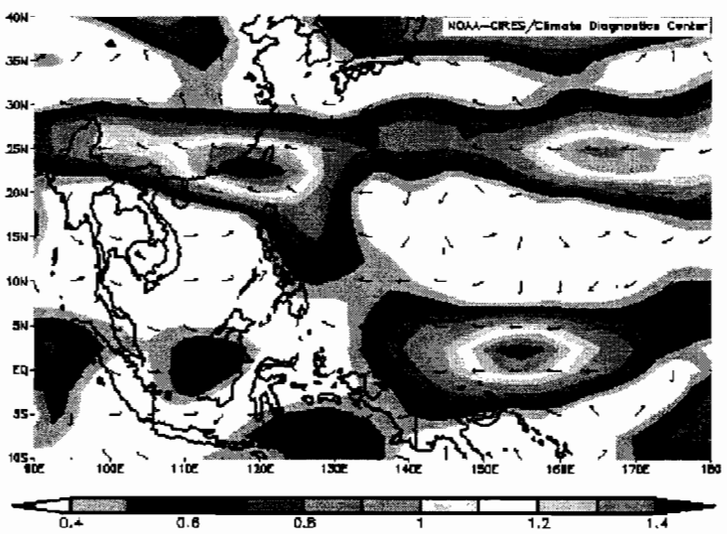

Composite analyses are applied and composite maps of mid-tropospheric wind anomalous patterns in the fall (September to November) are constructed for years with N below and higher than normal respectively (Figure 7).

An anomalous cyclonic circulation over the SCS and an anomalous anticyclonic circulation in eastern China in the case of N higher than normal are observed. This results in a strong anomalous steering current towards the coast of southern China, bringing more tropical cyclones towards Hong Kong. For the years with N below normal, the anomalous steering current over the northern part of the SCS and the western North Pacific Ocean east of Luzon is westerly. Tropical cyclones occurring over these areas are therefore less likely to affect Hong Kong.

Figure 8a. **500 hPa vector wind anomaly composite maps in summer for (a) El Niño years (b) La Niña years. (The arrow indicates the direction of wind anomaly and the colour scale represents the magnitude of wind anomaly in ms^{-1}. Image is provided by NOAA-CIRES Climate Diagnostic Center, Boulder, Colorado from the web site at http://www.cdc.noaa.gov/).**

(a) El Niño summer

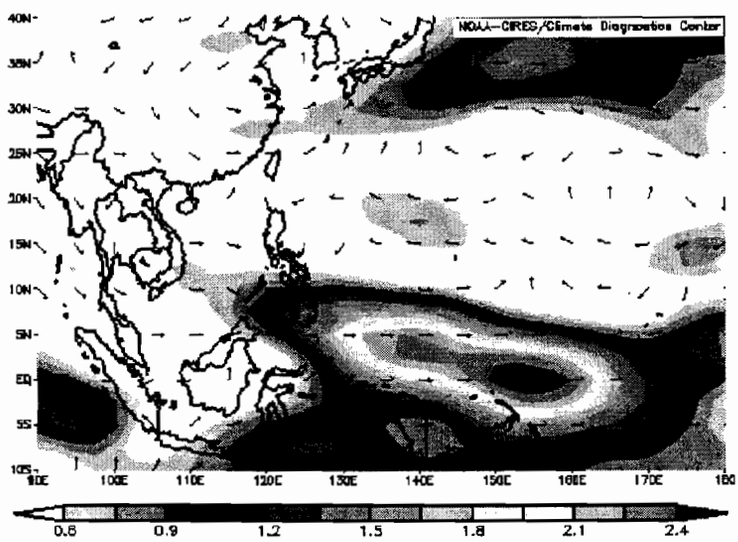

(b) La Niña summer

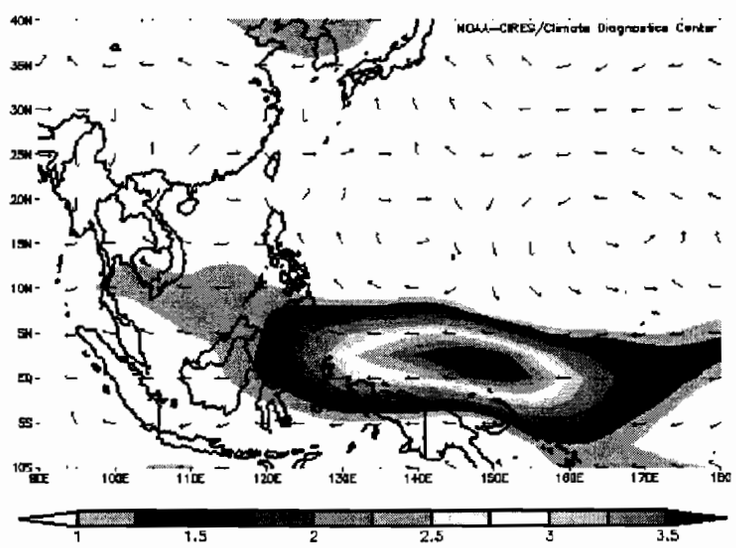

Composite maps are also constructed to see if there are distinct differences in atmospheric steering flow pattern between El Niño and La Niña years. Figure 8 shows a marked contrast in the mid-tropospheric wind anomalous patterns near the SCS between El Niño and La Niña years. This contrast is more distinct in Figure 8 (c) and (d), the fall (September to November), than in Figure 8 (a) and (b), the summer (June to August). In the fall, anomalous anticyclonic and cyclonic circulation patterns develop in the SCS and eastern China respectively for El Niño events. For La Niña events, anomalous cyclonic and anticyclonic circulations are observed respectively in the SCS and eastern China.

Figure 8b. **500 hPa vector wind anomaly composite maps in fall for (c) El Niño years (d) La Niña years. (The arrow indicates the direction of wind anomaly and the colour scale represents the magnitude of wind anomaly in ms^{-1}. Image is provided by NOAA-CIRES Climate Diagnostic Center, Boulder, Colorado from the web site at http://www.cdc.noaa.gov/).**

(c) El Niño fall

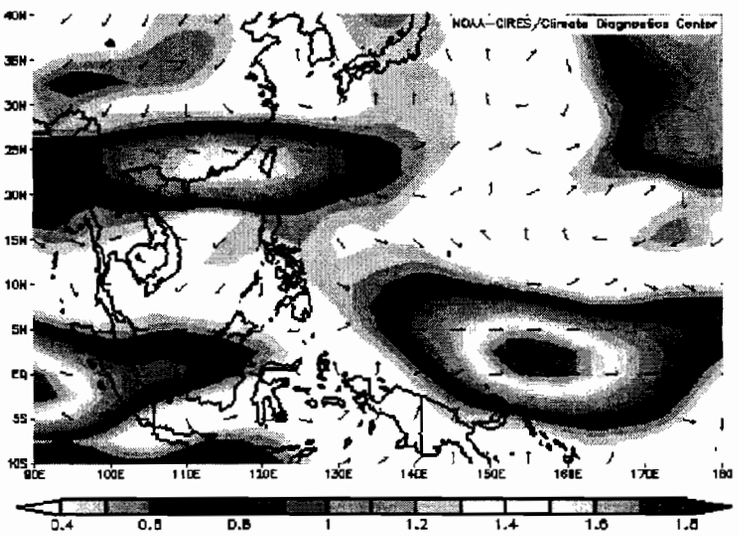

(d) La Niña fall

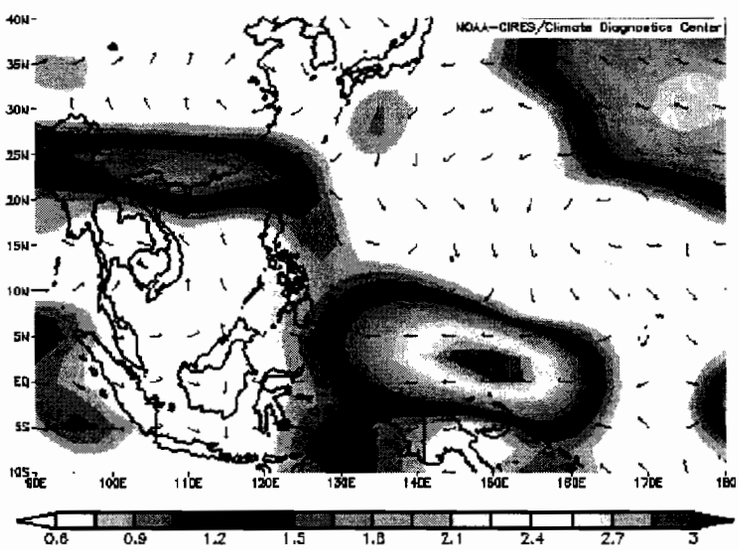

These result in opposite anomalous steering flows in the areas around the Luzon Strait and the northern part of SCS for the two events. The anomalous mid-tropospheric circulation pattern for El Niño years reduces the steering of tropical cyclones towards the region near Hong Kong and thus reduces the number of tropical cyclones affecting Hong Kong. In the La Niña years, the anomalous steering flow over the Pacific east of Luzon and in the northern part of the SCS is easterly. Tropical cyclones which form over these sea areas are more likely to be steered towards Hong Kong.

Summary

Tropical cyclone activity has been found to be significantly correlated with SSTAs and ENSO events. The annual number of tropical cyclones affecting Hong Kong is well correlated with the sea surface temperature anomaly in the Niño-3.4 regions. The higher the SSTAs in the equatorial Central and Eastern Pacific, the lower the number of tropical cyclones affecting Hong Kong. This result corroborates those of the study by Liu (2000) for tropical cyclones making landfall in Guangdong. The annual number of tropical cyclones is predominantly less than normal for EN(0) years and EN+1 years. For LN(0) and LN+1 years, predominantly more tropical cyclones affect Hong Kong. No conclusion can be drawn for EN-1, LN-1 and LN+2 years.

Marked changes in the mean tropical cyclone genesis locations as well as the mid-tropospheric steering flow patterns over the northern part of the South China Sea are associated with ENSO events. Such changes are the intermediate factors affecting the tropical cyclone activity in Hong Kong.

Acknowledgement

The material presented in this paper was originally presented at the *Workshop on the Network System for Monitoring and Predicting ENSO Event and Sea Temperature Structure of the Warm Pool in the Western Pacific Ocean*, Macau, China, 5-7 February, 2002.

References

Chan, J.C.L. (1985) Tropical cyclone activity in the northwest Pacific in relation to the El Niño/Southern Oscillation phenomenon. *Mon. Wea. Rev.*, **113**, 599-606.

Chen, T.C., S.P. Weng, N. Yamazaki and S. Kiehne (1998) Interannual variation in the tropical cyclone formation over the western North Pacific. *Mon. Wea. Rev.*, **126**, 1080-1090.

Kalnay, E., and Coauthors (1996) The NCEP/NCAR 40-year reanalysis project. *Bull. Amer. Meteor. Soc.*, **77**, 437-471.

Lander, M.A. (1994) An exploratory analysis of the relationship between tropical storm formation in the western North Pacific and ENSO. *Mon. Wea. Rev.*, **122**, 6636-651.

Liu, C.X. (2000) Study of formation causes for anomalies of annual tropical cyclone frequency in Guangdong. *Research on short-term climatic prediction in Guangdong Province*, Meteor. Press, 344 pp (in Chinese).

T.C. Lee & W. M. Leung

Hong Kong Observatory, 134A Nathan Road, Kowloon, Hong Kong

Performance of Multiple-model Ensemble Techniques in Tropical Cyclone Track Prediction

Abstract

The performance of the EW multiple model ensemble method in forecasting tropical cyclone tracks in the South China Sea (SCS) and the western North Pacific (WNP) for the 3-year period from 1999 to 2001 is evaluated and compared with the forecasts of the three global models. Results show that the multiple model ensemble method using the EW scheme outperformed all individual models in TC track prediction in 1999-2001. Reductions in 24-, 48-, and 72-hour forecast errors are about 7 percent, 17 percent and 19 percent respectively. The HKO's subjective TC track forecast in 2002 was also verified to investigate the effect of the ensemble method on operational TC track forecast. The use of the EW multiple model ensemble method results in significant improvement of the performance of HKO's official TC forecast. Possible improvements in the ensemble method using weighting schemes based on initial position error and 12-hour forecast errors are briefly discussed.

Introduction

In recent years, weather forecasting centres have increasingly adopted single model or multiple model ensemble methods to optimize tropical cyclone (TC) predictions. For the single model approach, ensemble members are generated from a single numerical model using different initial conditions representing the uncertainty of the analysis (Aberson, S.D. *et al.*, 1995; Zhang, Z. & Krishnamurti, T.N., 1997; and Cheung, K.K.W., 2001). The multiple model ensemble method makes simple the averaging of the forecast outputs of several models from different centres (Goerss, J.S. (2000); and Aberson, S.D., 2001;).

The Hong Kong Observatory (HKO) began in 1999 to experiment with a multiple model ensemble method based on the equally weighted (EW) average of the forecast positions of several global numerical models. The forecast positions are extracted from prognostic products of the European Centre for Medium-Range Forecasts (ECMWF), the Japan Meteorological Agency (JMA) and the UK Meteorological Office (UKMO). In view of its superiority over the forecasts of individual models, the EW multiple model ensemble method was put into operational use in 2002. Official tropical cyclone forecast tracks followed closely the multiple model ensemble forecast unless there were large discrepancies amongst the model forecasts.

In the study presented in this paper, the performance of the EW multiple model ensemble method in forecasting tropical cyclone tracks in the South China Sea (SCS) and the western North Pacific (WNP) for the 3-year period from 1999 to 2001 was evaluated and compared with the forecasts of the three global models. The HKO's subjective TC track forecast in 2002 was also verified to investigate the effect of the ensemble method on operational TC track forecast. Lastly, possible improvements in the ensemble method using weighting schemes based on initial position error and 12-hour forecast errors were briefly discussed.

Data Sources

Model forecast TC positions within the SCS and WNP (0-45°N, 100-180°E) for the period of 1999-2001 were used in this study. The forecast TC positions of the ECMWF and JMA models were determined from the surface prognoses as the point of minimum mean sea-level pressure (MSLP) identified by overlapping parabolic interpolation (Manning, K.W. & Haagenson, P.L., 1992). The forecast TC positions of the UKMO global model are extracted from the TC guidance of UK Meteorological Office (Bracknell) received *via* the WMO Global Telecommunication System. Table 1 lists the forecast start times and forecast intervals of the model outputs available to HKO in the period 1999-2001.

Table 1 **Details of model run schedules and forecast intervals of TC forecast products available to HKO in 1999-2001.**

Models	Forecast start time	Forecast intervals
ECMWF	12 UTC	24-hour
JMA	00 & 12 UTC	12-hour
UKMO	00 & 12 UTC	12-hour (24-hour before July 2001)

As only the prognoses for 12 UTC (but not 00 UTC) were available from ECMWF, the 36-, 60-, and 84-hour TC forecast positions were obtained by linear interpolation of the forecast positions in the preceding 12 UTC ECMWF model run. They were used to calculate the 24-, 48-, and 72-hour ensemble forecast positions for 00 UTC. The 00 and 12 UTC TC forecast positions of the three models and those of the ensemble forecasts were verified against HKO's 'best track' positions. Verification was conducted only for those cases in which prognostic data from all three global models were available. The HKO's 24- and 48-hour subjective TC track forecasts in 2002 were also verified against the "best track" within Hong Kong's area of responsibility for issuing tropical cyclone warnings for shipping (10-30°N, 105-125°E).

Performance of Equally Weighted Ensemble Method Against Individual Models

The multiple model ensemble method currently used by HKO assigns equal weights to the forecast TC positions of the three models to determine the average position. Table 2 shows the mean and standard deviations of the 24-, 48-, and 72-hour forecast errors of the EW ensemble method and those of the individual models in 1999-2001.

It can be seen that the mean forecast errors of the JMA and UKMO models were similar for all forecasting periods. The mean forecast error of the ECMWF model was comparatively larger. The poorer performance of the ECMWF model, especially for the 24-hour forecast period, may be partly due to the fact that lower resolution (2.5° * 2.5°, in contrast to JMA's 1.25° * 1.25°) forecast products were available for this study and that 00 UTC forecast positions were obtained by linear interpolation of the forecasts of the preceding 12 UTC model run.

Comparing with the forecast errors of individual models, the EW ensemble method outperforms the best of the three models in 1999-2001. The overall mean forecast error of the EW ensemble method at 24, 48, and 72 hours is about 7%, 17% and 19% less than the mean forecast errors of the best of the individual models respectively. Moreover, the standard deviation of forecast errors of the ensemble method is smaller than those of the individual models, especially for the 72-hour forecast. These results agree with the findings of recent studies (Goerss, J.S., 2000); and Lam, H., & M.H. Ma, 2002) in which different combination of models and shorter data periods were used.

Performance of HKO's Subjective Forecast in 2002

In view of the encouraging results mentioned in the section above, HKO put the EW multiple model ensemble method into operational use in 2002. Operational guidance has also been established to assist forecasters in formulating the official TC forecast track using the ensemble model as a primary guidance. Forecasters can exercise their judgment to apply meteorological reasoning to adjust the subjective forecast track if the models give widely divergent track forecasts.

To assess the effect of the ensemble method on HKO's TC track forecasting skill, the errors of the HKO's subjective forecasts in 2002 were compared with those obtained by the climatology-persistence (CLIPER) method (Bell, G. J., 1962). In general, the skill of a particular forecast relative to the CLIPER forecast is represented by the skill score, where:

$$\text{skill score} = \frac{(\text{CLIPER error - error of a particular forecast})}{\text{CLIPER error}} \times 100\%$$

The skill score is therefore a measure of normalized improvement over CLIPER. Positive skill indicates that the forecast outperforms the CLIPER forecast and negative skill indicates otherwise.

Table 3 Summary of mean forecast errors and Skill Scores of the HKO subjective forecast and EW ensemble forecast in 2002

Forecast Hours	**24 hours**		**48 hours**	
Forecast	HKO	Ensemble	HKO	Ensemble
Mean Forecast Error (km)	119	97	212	165
Skill Score	50%	59%	55%	65%
5 Year (1997-2001) Mean Error of HKO subjective forecast (km)	178		341	

Table 3 shows the mean forecast errors and skill scores of the HKO subjective forecast and EW ensemble forecast in 2002. There is a significant reduction in the 24- and 48-hour mean forecast errors of the HKO subjective forecast when compared with the corresponding mean forecast errors in the period 1997-2001. Also, the skill score of the 48-hour subjective forecast of HKO reaches an all-time high of 55% in more than two decades (Figure 1). This shows that the skill of ensemble forecast has translated into a noticeable improvement in HKO's official TC forecast.

Possible Improvement in Multiple Model Ensemble Method

As discussed in an earlier section, the UKMO and JMA models had, on average, smaller errors in TC track forecast when compared with the ECMWF model in 1999-2001. However, for 24-hour forecast, there were still over 30% of the cases in which the ECMWF model performed better than the JMA and/or UKMO models (Figures 2 and 3).

Figure 1 Skill relative to CLIPER of the 24- and 48-hour HKO subjective TC track forecast, 1980-2002 (Area : 10-30°N, 105-125°E).

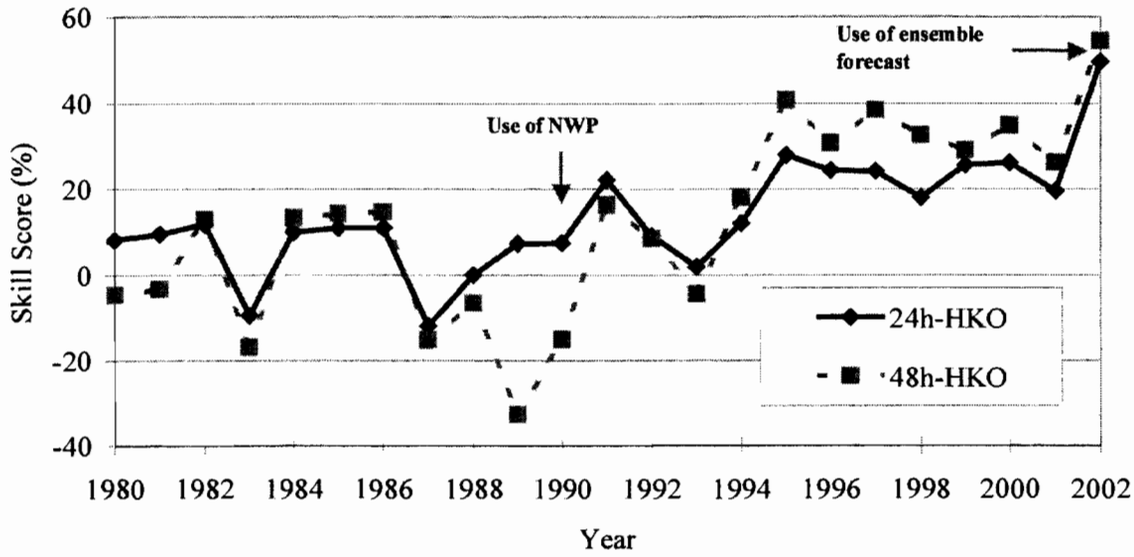

Figure 2 Scatter plot of 24-hour forecast error of JMA against EMCWF.

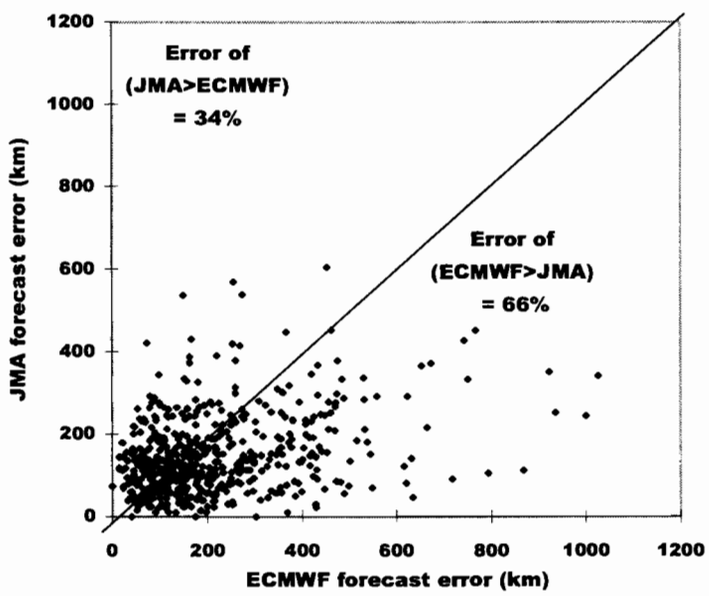

Figure 3 **Scatter plot of 24-hour forecast error of UKMO against EMCWF.**

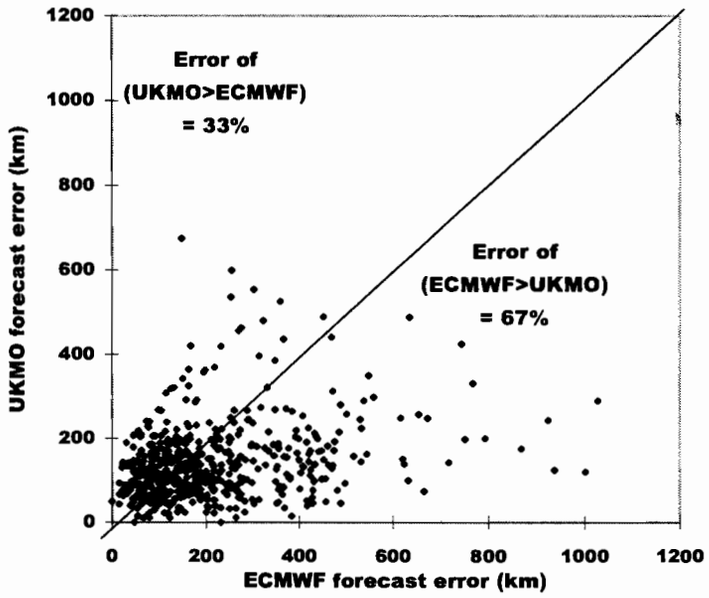

The percentages for 48- and 72-hour forecasts even increased to some 40 percent and 50 percent respectively. This means that none of the three models is superior to the other two on all occasions. It should therefore be possible to reduce the ensemble forecast error by assigning more weight to the models with better performance on a case-by-case basis. Lee, T.C., and Wong, M.S. (2002) recently tested two ensemble weighting schemes based respectively on the direct position error of (a) initial position (DPE00) and (b) the 12-hour forecast position error (DPE12) to see if more accurate ensemble forecasts could be made. The results (Table 4) show that while the EW scheme and DPE00 scheme have similar performance, the DPE12 scheme can improve the ensemble forecasts in the 24- and 48-hour forecast periods.

Table 4 **Mean and standard deviations of 24-, 48-, and 72-hour forecasts of the EW, DPE00, and DPE12 schemes**

Forecast period (hr)	EW Mean error (standard deviation)	DPE00 Mean error (standard deviation)	DPE12 Mean error (standard deviation)
24	130 (86)	123 (80)	108 (74)
48	213 (153)	214 (148)	204 (139)
72	308 (204)	320 (212)	308 (190)

Conclusion

This study has shown that the multiple model ensemble method using the EW scheme outperformed all individual models in TC track prediction in 1999-2001. Reductions in 24-, 48-, and 72-hour forecast errors are about 7 percent, 17 percent and 19 percent respectively. The use of the EW multiple model ensemble method has resulted in significant improvement of the performance of HKO's official TC forecast. It is possible to further improve the performance of the ensemble forecast by using a different weighting scheme based on the 12-hour forecast position errors of individual members of the ensemble.

Acknowledgement

The material presented in this paper was originally presented at the *35th Session* of the *WMO/ESCAP Typhoon Committee*, Chiang Mai, Thailand, 19-2 November, 2002.

References

Aberson, S.D. (2001). The ensemble of tropical cyclone track forecasting models in the North Atlantic Basin (1976-2000), *Bull. Amer. Meteor. Soc.,* **82** , 1895-1904.

Aberson, S. D., Lord, S. J., DeMaria, M., & Tracton, M. S., (1995). Short-range ensemble forecasting of hurricane tracks. In *Preprints, 21st Conf. Hurr. Trop. Meteorol., Miami, Am. Meteorol. Soc.*, 290-292.

Bell, G. J. (1962). Predicting the movement of tropical cyclones in the region of the China sea. Proceedings of the Inter-Regional Seminar on Tropical Cyclones, Tokyo, 1962. (Techn. Rep. JMA, No. 21).

Cheung, K. K. W., (2001). A review of ensemble forecasting techniques with a focus on tropical cyclone forecasting. *Meteorol. Appl.* 8, 315-332.

Goerss, J. S. (2000). Tropical cyclone track forecasts using an ensemble of dynamical models. *Mon. Wea. Rev.*, **128**, 1187-1193.

Lam, H., & Ma, M. H. (2002). A review of the use of NWP models for tropical cyclone track prediction at Hong Kong Observatory in 2001 (in Chinese only). 16th Hong Kong-Guangdong-Macau Symposium On Met. Science & Technology (Guangzhou, 30 to 31 Jan 2002).

Lee, T. C., and Wong, M. S. (2002). The use of multiple model ensemble techniques in tropical cyclone track forecast at the Hong Kong Observatory. Hong Kong Observatory internal communication, 2002.

Manning, K. W. & Haagenson, P. L. (1992). Data ingest and objective analysis for the PSU/NCAR modeling system: Programs DATAGRID and RAWINS. *NCAR Technical Note, NCAR/TN-376+LA*, 209 pp.

Zhang, Z., and Krishnamurti, T. N., (1997). Ensemble forecasting of hurricane tracks. *Bull. Am. Meteorol. Soc.*, **78**: 2785-2795.

P.W. Chan and K.K. Yeung

Hong Kong Observatory, 134A Nathan Road, Kowloon, Hong Kong

Experimental Use of Weather Buoy in Windshear Monitoring at the Hong Kong International Airport

Introduction

This paper describes the introduction of a weather buoy near the Hong Kong International Airport (HKIA) and presents its applications to windshear monitoring and alerting for aircraft flying in and out of the airport.

The HKIA was opened in July 1998. There are two parallel runways orientated in 070-250 degree direction (Figure 1). It is located on a reclaimed island surrounded by waters on three sides. To the south of it, the rather mountainous Lantau Island has hills reaching 950 m above mean sea level.

The land-sea interaction and the hilly terrain often produce complex airflow patterns in and around the airport. A number of windshear events are known to have resulted from the setting in of sea breeze (Lee and Shun, 2002) and from wind disturbances caused by cross-mountain flow (Lau and Shun, 2000).

In aviation meteorology, windshear refers to a sustained change in headwind or tailwind, resulting in changes in the lift to an aircraft. Apart from sea breeze and cross-mountain flow in the airport environment, windshear can also arise from the passage of a cold front, or a gust front associated with thunderstorms (Lau et al., 2002). For Hong Kong, in the period from July 1998 to December 2001, 0.14% of all flights in and out of the airport reported significant windshear, i.e. windshear reaching 15 knots or more.

In running the windshear and turbulence alerting service at HKIA, the Hong Kong Observatory (HKO) operates a network of land-based automatic weather stations around the airport (Figure 1). HKO also operates remote-sensing equipment including a Terminal Doppler Weather Radar (TDWR) and wind profilers for monitoring the weather and wind pattern there. The radar covers severe weather reasonably well, including thunderstorms and microbursts. An infrared LIDAR (Light Detection And Ranging) system was installed in mid-2002 to cover fine weather situations, and its performance will be evaluated.

HKO installed a weather buoy over the waters to the west of the airport in December 2001. This is the first time a weather buoy was deployed in Hong Kong. The purpose is to fill in a data void over the area and to provide 'ground' truth complementing the remote-sensing equipment.

Figure 1 Map of HKIA and the surrounding areas. The weather buoy and the other weather stations around the airport are indicated by dots. Terrain contours are in 100-m intervals.

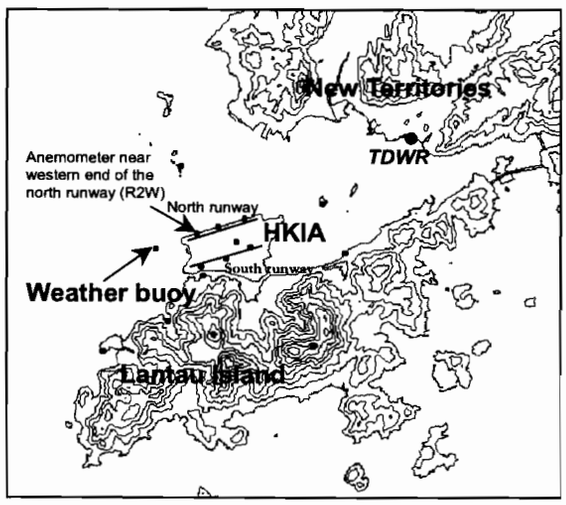

Figure 2 The first weather buoy in Hong Kong.

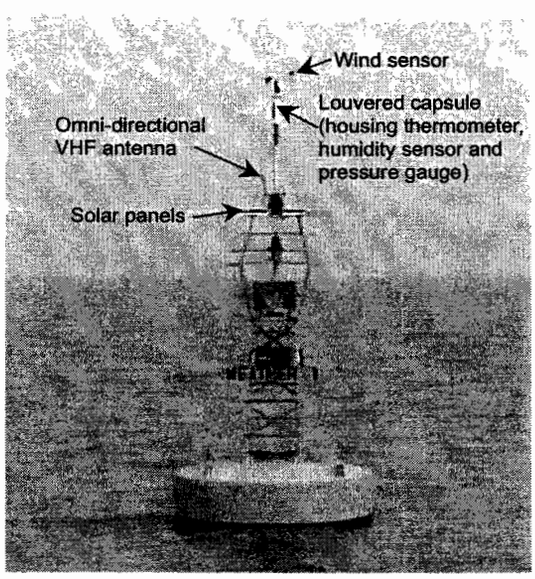

Equipment Set-Up

Figure 2 shows the weather buoy. Its hull is adapted from a common type of marine navigation buoy in Hong Kong. An automatic weather station specifically designed for use on a buoy is mounted at the top, with a propeller-type wind sensor at the highest point (about 7 m above sea surface), and beneath it a louvered capsule housing a thermometer, a humidity sensor and a pressure gauge.

Weather measurements are sent out every 10 seconds to the HKO office at the airport. This is achieved by means of an omni-directional VHF radio antenna alongside the weather equipment.

Time-stamping of the weather data is carried out using a Global Positioning System (GPS) receiver on-board, which provides regular synchronization for the weather equipment. The stated timing accuracy is within 50 nanoseconds of GPS satellite clocks.

The buoy operates solely on solar energy. It is equipped with 6 units of 20-Watt solar panels to support the weather measurements, data transmission every 10 seconds, as well as the navigation light. The battery voltage is also regularly radioed back to enable monitoring of its status.

The performance of the weather buoy has been satisfactory with no major problem since its commissioning in late 2001. So are the solar panels which have maintained the continuous operation of the buoy for up to a week during cloudy spells.

Applications to windshear monitoring and alerting

For monitoring windshear, real-time wind data from the relevant stations are used to estimate the change in the headwind. As an example, for an aircraft approach towards the north runway from the west, the component of wind at the weather buoy along the direction of the north runway is subtracted from the corresponding value of the anemometer near the western end of the runway (R2W), giving a value indicative of the horizontal windshear. A resulting vector pointing to 070 (250) degrees implies a loss (gain) of headwind or a gain (loss) in tailwind for the aircraft. Likewise, the difference in headwind between a hill station and a coastal station gives an indication of the vertical windshear.

After detailed studies, two alert levels based on headwind differences were established:

(a) 10-knot difference – significant windshear is probable, and the forecaster should be on the alert;
(b) 15-knot difference – significant windshear is very probable, and the forecaster should actively consider the issuance of windshear alerts taking into account other meteorological data.

Since its commissioning in late 2001, the weather buoy has demonstrated a capability for more timely alerting of significant windshear under several different weather conditions. Some examples are given below.

Sea breeze

At the airport, sea breeze is typically characterized by westerly winds setting in over the waters west of the airport (Cheng, 2002). With easterly winds normally prevailing, the opposing westerly/easterly winds in the vicinity of the sea breeze front sometimes result in significant windshear.

An example of sea-breeze induced windshear occurred on 31 January 2002. Under the influence of an area of high pressure centred over east China, the weather was generally fine in Hong Kong on that day with easterly winds prevailing (Figure 3). As early as 10 a.m. (Hong Kong time = UTC + 8 hours), temperatures at the airport already rose above the sea surface temperature of 17 degrees, favoring the formation of sea breeze.

Figure 3. Surface weather chart at 8 a.m., 31 January 2002.

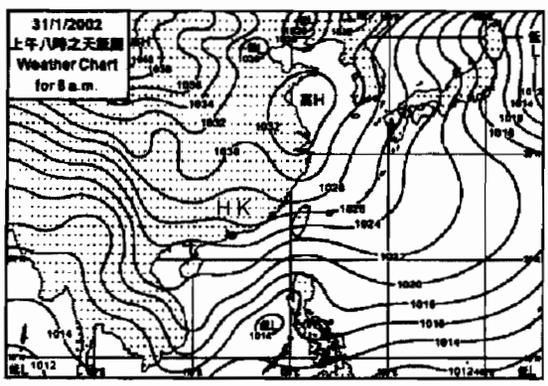

The movement of the sea breeze front was established by using wind velocity data of TDWR, the buoy and the runway anemometers (Figure 4). It can first be analyzed from this data set around noon. The front moved northeastwards past the weather buoy at about 1 p.m. and reached its eastern-most location two hours later over the western part of the airport. The sea breeze front retreated to the west gradually in late afternoon.

Figure 4. Wind distribution around the airport at 1 p.m., 31 January 2002. Locations and movement of the sea breeze front are overlaid on the map.

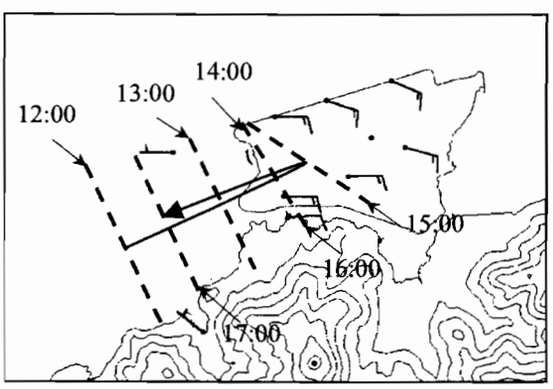

Figure 5. **Wind difference between R2W anemometer and the weather buoy, with arrows indicating the times of actual windshear reports by aircraft landing at the north runway from the west.**

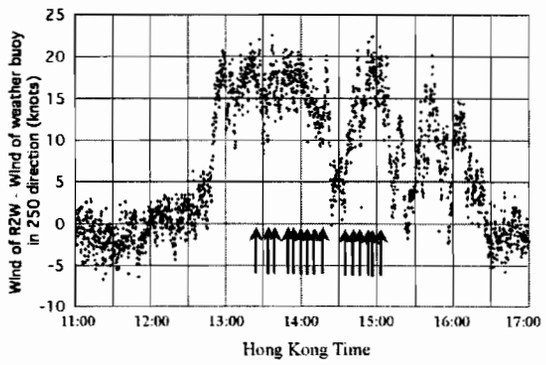

The passage of sea breeze front resulted in the change of wind direction of the buoy from easterly to westerly at about 12:45 p.m. As easterly wind still prevailed over the airport, the wind difference between the buoy and R2W anemometer in the 250 direction (*i.e.* along runway) increased significantly to +20 knots at that time (Figure 5). It stayed above 15 knots occasionally until around 3:45 p.m. During this period, 15 significant windshear reports were received from aircraft landing at the airport from the west.

In the first six months of 2002, there were altogether 38 reports of significant, sea-breeze related windshear by aircraft landing from west of the north runway of the airport. By applying the rules described in the beginning of this section, it was found that windshear alerts could be issued for 30 reports in a more timely manner, with advance alerting possible from 15 to 30 minutes earlier. This result represents a success rate of 79%.

Passage of A GUST front

In the morning of 24 March 2002, a cold front moved southwards and crossed the southern coast of China (Figure 6), with bands of rain associated with the front affecting Hong Kong during the day. From the weather radar pictures (not shown), a band of radar echoes with NNE to SSW orientation moved across Hong Kong in the early afternoon. The prevailing easterly wind over the territory gave way to northerly wind at the same time. As it progressed eastwards, the gust front assumed a more or less similar orientation, i.e. NNE to SSW (Figure 7).

At the airport, the wind at the weather buoy backed to northerly abruptly upon the arrival of the gust front. The wind difference between the buoy and R2W anemometer rose abruptly to +20 knots in the space of 5 minutes (Figure 8). This is consistent with a windshear report of 15-knot wind gain by an aircraft landing at the north runway from the west around that time. With the passage of the gust front, northerly wind prevailed over the whole airport and the surrounding area and significant windshear no longer occurred.

Figure 6. Surface weather chart at 8 a.m., 24 March 2002.

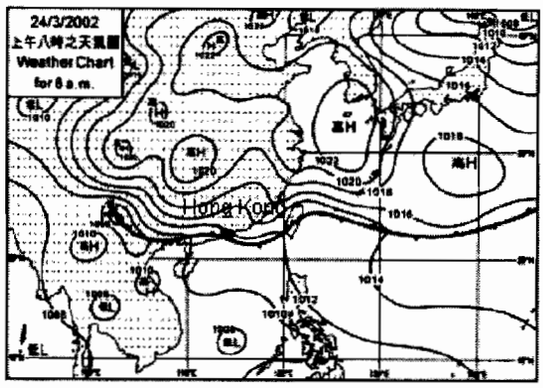

Figure 7. Winds around the airport at 2:25 p.m., 24 March 2002. The gust front's locations at various times are indicated by broken lines.

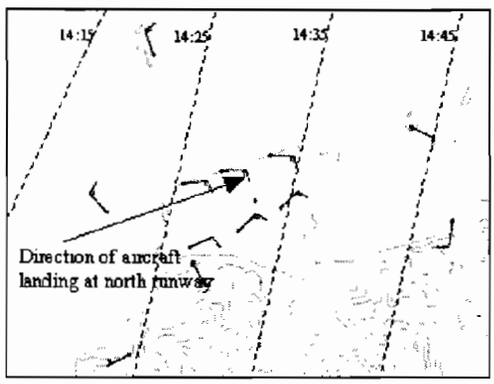

Figure 8. Wind difference between R2W anemometer and the weather buoy between 2 and 3 p.m., 24 March 2002. The time of actual windshear report is indicated by an arrow.

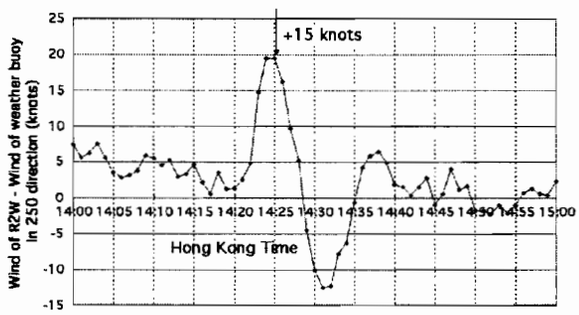

Wind disturbance downwind of terrain

When the prevailing wind of Hong Kong is from east through southeast, HKIA lies downwind of Lantau Island. Observational studies revealed that the low-level atmospheric flow downwind of the island could be quite complicated in certain weather conditions (Lau *et al.*, 2002).

An example of terrain-induced windshear occurred in the afternoon of 18 January 2002. Synoptically, a ridge of high pressure ahead of a cold front over south China brought easterlies to the coastal area on the surface (Figure 9), with winds aloft veering to the south on hilltops of Lantau (about 900 m above mean sea level).

Figure 9. Surface weather chart at 8 a.m., 18 January 2002.

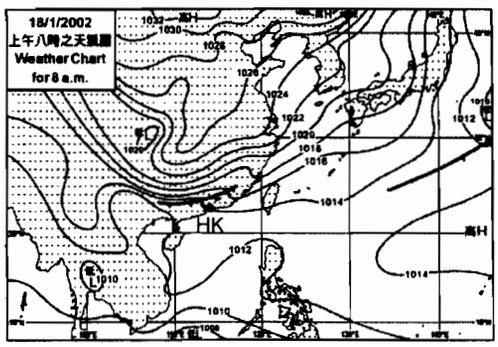

Figure 10. Time sequence of wind observations between 3:15 p.m. and 4 p.m., 18 January 2002.

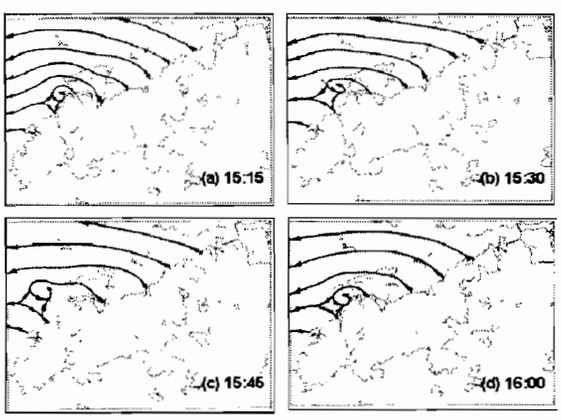

Figure 10 shows a time sequence of the wind observations depicting the local wind disturbances near the airport during the period of 3:15 p.m. to 4 p.m. While winds over the airport remained generally easterly, the weather buoy reported winds changing from northeasterly to northwesterly, then southerly and finally northeasterly. This successive change in wind direction at the buoy, against rather steady winds in the background, suggests the existence of small vortices one by one, over the western part of the airport, and their subsequent movement to the northwest. The small vortices brought about changes in the headwind experienced by the aircraft.

The wind difference between the buoy and R2W anemometer is shown in Figure 11. Four aircraft reported encountering windshear of -15 to +20 knots during the period while landing at HKIA from the west. A windshear alert had been issued in advance and we received the compliment from one of the pilots that the alert had got him well prepared to deal with the windshear encounter.

Figure 11. Wind difference between R2W anemometer and the weather buoy on 18 January 2002. The times of actual windshear reports are indicated by arrows.

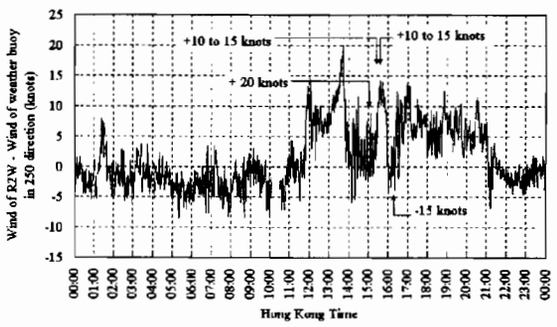

Conclusion

The HKO deployed the first weather buoy in Hong Kong in late December 2001 to supplement the existing network of land-based automatic weather stations. The buoy is strategically located west of HKIA to make weather measurements in the data-sparse sea area and to monitor the airflow for aircraft moving west of the airport. It transmits weather data in real-time once every 10 seconds.

The buoy has demonstrated its capability in the monitoring of windshear in different weather conditions, including sea breeze, passage of gust fronts and wind disturbance downwind of Lantau terrain. The wind difference between the buoy and the R2W anemometer is used to assess the likelihood of significant windshear over the western approach/departure corridor of the airport. Two alert levels (10-knot and 15-knot wind differences) were found to provide very helpful guidance in the timely issuance of windshear alerts. For instance, for sea-breeze induced windshear alone, the use of the 15-knot alert level is capable of catching about 79% of the significant windshear reports by aircraft landing from west of the airport in the first six months of 2002.

Acknowledgement

The material presented in this paper was originally presented at the *Eighteenth Session* of the *WMO/IOC Data Buoy Co-operation Panel and Scientific and Technical Workshop*, Trois Ilets, Martinique, France, 14-18 October, 2002.

References

Cheng, C.M., (2002) Sea-breeze Induced Windshear at Chek Lap Kok, Hong Kong, Technical Note No. 103, Hong Kong Observatory, 21 pp.

Lau, S.Y. and C.M. Shun (2000) Observation of terrain-induced windshear around Hong Kong International Airport under stably stratified conditions. *Preprints, 9th Conf. on Mountain Meteorology,* Amer. Meteor. Soc., 93-98.

Lau, S.Y., C.M. Shun and B.Y. Lee (2002) Windshear and Turbulence Alerting Service at the Hong Kong International Airport – A Review, Technical Note No. 102, Hong Kong Observatory, 19 pp.

Lee, S.M. and C.M. Shun (2002) Terminal Doppler Weather Radar Observation of Sea Breeze Interactions, submitted to *Meteorological Applications.*

HONG KONG METEOROLOGICAL SOCIETY

INFORMATION FOR CONTRIBUTORS TO THE BULLETIN

Technical or research articles, as well as reviews and correspondence of a topical nature are welcome. In general contributions should be short, although exceptions may be made by prior arrangement and at the sole discretion of the Editorial Board. Copyright of material submitted for publication remains that of the author(s). However, any previous, current, or anticipated future use of such material by the author must be stated at the time of submission. All existing copyright materials to be published must be cleared by the contributor(s) prior to submission.

Manuscripts must be accurate and preferably in the form of a diskette containing an electronic version in one of the common word processing formats. WORD is preferred but others are also acceptable. Whether or not an electronic version is submitted, two complete manuscript copies of the articles should be submitted. These should be preceded by a cover page stating the title of the article, the full name(s) of the author(s), identification data for each author (position and institution or other affiliation and complete mailing address). An abstract of about 150 words should be included. Manuscripts should be double-spaced, including references, single-side only on A4 size paper with a 2.5 cm margin on all sides, and be numbered serially. All references should be arranged in alphabetical and, for the same author, chronological order. In the text they should be placed in brackets as (Author'(s) name(s), date). In the reference list at the end the Author'(s) name(s) and initials followed by the date and title of the work. If the work is a book this should be followed by the publisher's name, place of publication and number of pages; or, if a journal article, by the title of the periodical, volume and page numbers.

Submission of electronic versions of illustrations is encourage. Originals of any hardcopy illustrations submitted should be in black on tracing material or smooth white paper, with a line weight suitable for any intended reduction from the original submitted size. Monochrome photographs should be clear with good contrasts. Colour photographs are also accepted by prior arrangement with the Editorial Board. Originals of all illustrations should be numbered consecutively and should be clearly identified with the author'(s) name(s) on the back. A complete list of captions printed on a separate sheet of paper.

All submitted material is accepted for publication subject to peer review. The principal author will be sent comments from reviewers for response, if necessary, prior to final acceptance of the paper for publication. After acceptance the principal author will, in due course, be sent proofs for checking prior to publication. Only corrections and minor amendments will be accepted at this stage. The Society is unable to provide authors with free offprints of items published in the Bulletin, but may be able to obtain quotations from the printer on behalf of authors who express, at the time of submission of proofs, a desire to purchase a specified number of offprints.

Enquiries and all correspondence should be addressed to the Editor-in-Chief, Hong Kong Meteorological Society Bulletin, c/o Department of Geography, The University of Hong Kong, Pokfulam Road, Hong Kong. (*Tel. +(852) 2859-7022; Fax. +(852) 2559-8994 or 2549-9763; email: billkyle@hkucc.hku.hk.*

香港氣象學會

HONG KONG METEOROLOGICAL SOCIETY

Bulletin

Volume 12, Numbers 1/2, 2002

SINGLE COPY PRICE: HK$ 150

(for subscription rates see inside front cover)

CONTENTS